

An Arbitrary High Order Discontinuous Galerkin Method for Elastic Waves on Unstructured Meshes IV: Anisotropy

Josep de la Puente¹, Martin Käser², Michael Dumbser^{2,3}, Heiner Igel¹

¹ *Department of Earth and Environmental Sciences, Section Geophysics, Ludwig-Maximilians-Universität, München, Germany*

² *Laboratory of Applied Mathematics, Department of Civil and Environmental Engineering, University of Trento, Trento, Italy*

³ *Institut für Aerodynamik und Gasdynamik, Universität Stuttgart, Germany*

Accepted 1999 November 11. Received 1999 October 6; in original form 1999 August 3

SUMMARY

We present a new numerical method to solve the heterogeneous elastic anisotropic wave equation with arbitrary high order accuracy in space and time on unstructured tetrahedral meshes. Using the most general Hooke's tensor we derive the velocity-stress formulation leading to a linear hyperbolic system which accounts for the variation of the material properties depending on direction. This approach allows for the modeling of triclinic anisotropy, the most general crystalline symmetry class. The proposed method combines the Discontinuous Galerkin method with the ADER time integration approach using arbitrary high order derivatives of the piecewise polynomial representation of the unknown solution. In contrast to classical Finite Element methods discontinuities of this piecewise polynomial approximation are allowed at element interfaces, which allows for the application of the well-established theory of Finite Volumes and numerical fluxes across element interfaces obtained by the solution of derivative Riemann problems. Due to the ADER time integration technique the scheme provides the same approximation order in space and time automatically. Furthermore, through the projection of the tetrahedral elements of the physical space onto a canonical reference tetrahedron an efficient implementation is possible as many three-dimensional integral computations can be carried out analytically beforehand. A numerical convergence study confirms that the new scheme provides arbitrary high order accuracy even on unstructured tetrahedral meshes and shows that computational cost and storage space can be reduced by higher order schemes. Besides, we present a new Godunov-type numerical flux for anisotropic material and compare its accuracy with a computationally simpler Rusanov flux. Finally, we validate the new scheme by comparing the results of our simulations to an analytic solution as well as to Spectral Element computations.

Key words: anisotropy, Discontinuous Galerkin method, high order accuracy, tetrahedral meshes

1 INTRODUCTION

Anisotropic media are those whose material properties differ when measured in different directions. Exploration geophysics have for a long time paid attention to the anisotropic behaviour of the seismic waves in the soil in order to resolve, for example, crack alignment (Crampin, Chesnokov & Hipkin 1984; Helbig 1994) in hydrocarbon reservoirs. However, for many years anisotropy has been disdained as secondary effect in earthquake seismology. Now, as imaging of the Earth's deep structure is constantly improving, anisotropic material properties influencing seismic wave propagation have received more attention (Backus 1962; Cara 2002; Carcione 2002). In particular, it is essential to include anisotropy in high order accurate seismic simulation methods. Furthermore, it has been shown that strong stress regimes can enhance the anisotropy of materials (Sharma & Garg 2006) which requires the careful treatment of anisotropy in earthquake simulations and seismic wave propagation modeling at all scales.

In addition, the improvements of our knowlegde of the geological and geophysical properties of subsurface models in seismologically interesting regions often show highly complex geometries. This increasing complexity still presents a challenge for numerical methods based on regular, structured gridding. On the other hand, numerical methods on geometrically more flexible unstructured tetrahedral meshes until today could not provide high order accuracy. Therefore, most approaches were forced to find a compromise between preserving the complexity of the models and having highly accurate results.

In the past, many approaches describing anisotropic wave propagation have been developed. Early attempts aimed at the simplification of anisotropic effects for some weakly anisotropic media (Thomsen 1986; Song, Every & Wright 2001). Analytical and quasi-analytical solutions to simplified cases exist and ray theory can handle the problem to some extent (Červený 1972). However, when heterogeneous materials and complex geometrical structures are involved only three-dimensional, full wave form simulations are able to provide satisfying results. The most widely used method, the Finite Difference (FD) method, has successfully been extended from isotropic (Madariaga 1976; Virieux 1984; Virieux 1986) to anisotropic problems using staggered (Mora 1989; Igel, Mora & Rioulet 1995) or rotated staggered grids (Saenger & Bohlen 2004). However, both approaches are forced to interpolate stress and strain off-diagonal values as they are not defined in the same grid points. Pseudospectral (PS) methods (Carcione 1994; Tessmer & Kosloff 1994; Fornberg 1996; Igel 1999) have been extended to handle anisotropic material in (Carcione, Kosloff & Kosloff 1988; Tessmer 1995; Hung & Forsyth 1998). More recently, the Spectral Element Method (SEM) has considerably gained in popularity due to its accuracy and efficiency on deformable hexahedral elements (Komatitsch & Vilotte 1998; Komatitsch & Tromp 1999) and has also been further developed for anisotropic problems in (Seriani, Priolo & Pregarz 1995; Komatitsch, Barnes & Tromp 2000) and successfully been applied to the case of global seismic wave propagation in (Komatitsch & Tromp 2002). Recent attempts of incorporating anisotropy in fully unstructured grids in (Gao & Zhang 2006) represent an alternative approach.

Combining anisotropy with viscoelasticity is non-trivial task. Initial straightforward attempts have centered themselves in using complex values for each of the 21 independent coefficients of the general Hooke's tensor (Auld 1990). Alternative constitutive laws that solve the most general case based on different constitutive relations were developed by (Carcione & Cavallini 1994), based in the concept of eigenstresses and eigenstiffnesses, or (Carcione 1995) in which the concepts of mean and deviatoric stresses allow to build an attenuation implementation based on memory variables, making it both accurate and easy to implement in time-domain numerical modelling.

In this paper, we extend the Discontinuous Galerkin (DG) approach with a time integration approach using Arbitrary high order DERivatives (ADER) presented in (Käser & Dumbser 2006; Dumbser & Käser 2006; Käser, Dumbser, de la Puente & Igel 2006) to the three-dimensional anisotropic case for the most general triclinic crystalline symmetry class. The ADER-DG method provides arbitrary high order accuracy in space and time on unstructured tetrahedral meshes, which makes it very attractive when complicated model geometries are involved. To our knowledge the ADER-DG approach provides the first numerical scheme achieving high order polynomial approximation for anisotropic seismic wave propagation on three-dimensional unstructured meshes.

The paper is structured as follows. In Section 2 we present the linear hyperbolic system of the anisotropic seismic wave equations in velocity-stress formulation. In Section 3 we show the extension of the ADER-DG scheme to anisotropic material with particular focus on a new Godunov-type numerical flux. The coupling of anisotropy and viscoelastic attenuation is derived in Section 4. A convergence study is presented in Section 5 in order to validate the high order accuracy of the new ADER-DG scheme for anisotropic material. Finally, in Section 6 we demonstrate different application examples to confirm the performance of the proposed method by comparisons of our results with analytical solutions and results of the Spectral Element Method. Section 7 summarizes the work presented and provides concluding remarks.

2 ANISOTROPIC SEISMIC WAVE EQUATIONS

The most general linear elastic stress-strain relation can be expressed through a tensorial constitutive law (Hooke's Law), see e.g. (Stein & Wysession 2003), of the form

$$\sigma_{ij} = c_{ijkl} \varepsilon_{kl} \quad (1)$$

The entries of the fourth-order elasticity tensor c_{ijkl} can be reduced to 21 independent real coefficients in the most general case due to symmetry considerations. Using matrix notation, the stresses σ_{ij} and strains ε_{kl} are defined as vectors $\vec{\sigma} = (\sigma_{xx}, \sigma_{yy}, \sigma_{zz}, \sigma_{xy}, \sigma_{yz}, \sigma_{xz})^T$ and $\vec{\varepsilon} = (\varepsilon_{xx}, \varepsilon_{yy}, \varepsilon_{zz}, \varepsilon_{xy}, \varepsilon_{yz}, \varepsilon_{xz})^T$ and we can rewrite (1) using an anisotropic elastic matrix M_{ij} as

$$\vec{\sigma}_i = M_{ij} \vec{\varepsilon}_j, \quad (2)$$

which extended in more detail reads as

$$\begin{pmatrix} \sigma_{xx} \\ \sigma_{yy} \\ \sigma_{zz} \\ \sigma_{yz} \\ \sigma_{xz} \\ \sigma_{xy} \end{pmatrix} = \begin{pmatrix} c_{11} & c_{12} & c_{13} & 2c_{14} & 2c_{15} & 2c_{16} \\ c_{12} & c_{22} & c_{23} & 2c_{24} & 2c_{25} & 2c_{26} \\ c_{13} & c_{23} & c_{33} & 2c_{34} & 2c_{35} & 2c_{36} \\ c_{14} & c_{24} & c_{34} & 2c_{44} & 2c_{45} & 2c_{46} \\ c_{15} & c_{25} & c_{35} & 2c_{45} & 2c_{55} & 2c_{56} \\ c_{16} & c_{26} & c_{36} & 2c_{46} & 2c_{56} & 2c_{66} \end{pmatrix} \begin{pmatrix} \varepsilon_{xx} \\ \varepsilon_{yy} \\ \varepsilon_{zz} \\ \varepsilon_{yz} \\ \varepsilon_{xz} \\ \varepsilon_{xy} \end{pmatrix}. \quad (3)$$

Considering all 21 independent coefficients in M_{ij} we can represent a triclinic material, which is the most general case of anisotropy and includes as special cases all other crystalline symmetry classes, i.e. monoclinic, trigonal, tetragonal, orthorhombic, hexagonal, cubic and isotropic, as shown in (Nye 1985; Okaya & McEvelly 2003). Therefore, isotropy can be understood as the particular case in which $c_{11} = c_{22} = c_{33} = \lambda + 2\mu$, $c_{12} = c_{13} = c_{23} = \lambda$, $c_{44} = c_{55} = c_{66} = \mu$ and all other coefficients equal to zero. In non-isotropic cases

the actual values of the coefficients of the matrix M_{ij} in (3) depend on the orientation of the reference system we use. Certain anisotropic symmetry classes exhibit symmetry axes. Therefore, appropriate reference systems can be chosen in a way that structured grids are aligned to these symmetry axes. However, when modeling anisotropic wave propagation on unstructured meshes the reference coordinate system for each interface between two neighbouring elements, where numerical fluxes have to be computed, generally has a different orientation from the others and therefore a particular symmetry class can not be exploited. In fact, we generally have to treat a triclinic symmetry at each element interface due to its arbitrary orientation within an unstructured tetrahedral mesh. In the following, however, we consider the elastic properties of the anisotropic medium referring to the underlying physical coordinate system that also defines the orientation of stresses and strains or the physical coordinates of mesh nodes.

Combining the constitutive relation in (3) with the equations of motion, see e.g. (LeVeque 2002), leads to a complete partial differential equation system of the shape

$$\frac{\partial Q_p}{\partial t} + A_{pq} \frac{\partial Q_q}{\partial x} + B_{pq} \frac{\partial Q_q}{\partial y} + C_{pq} \frac{\partial Q_q}{\partial z} = 0, \quad (4)$$

where Q is the vector of the unknown stresses and velocities, i.e. $Q = (\sigma_{xx}, \sigma_{yy}, \sigma_{zz}, \sigma_{xy}, \sigma_{yz}, \sigma_{xz}, u, v, w)^T$. Note, that classical tensor notation is used, which implies summation over each index that appears twice. The matrices $A_{pq} = A_{pq}(\vec{x})$, $B_{pq} = B_{pq}(\vec{x})$, and $C_{pq} = C_{pq}(\vec{x})$ are the space dependent Jacobian matrices, with $p, q = 1, \dots, 9$, and are given through

$$A_{pq} = \begin{pmatrix} 0 & 0 & 0 & 0 & 0 & 0 & -c_{11} & -c_{16} & -c_{15} \\ 0 & 0 & 0 & 0 & 0 & 0 & -c_{12} & -c_{26} & -c_{25} \\ 0 & 0 & 0 & 0 & 0 & 0 & -c_{13} & -c_{36} & -c_{35} \\ 0 & 0 & 0 & 0 & 0 & 0 & -c_{16} & -c_{66} & -c_{56} \\ 0 & 0 & 0 & 0 & 0 & 0 & -c_{14} & -c_{46} & -c_{45} \\ 0 & 0 & 0 & 0 & 0 & 0 & -c_{15} & -c_{56} & -c_{55} \\ -\frac{1}{\rho} & 0 & 0 & 0 & 0 & 0 & 0 & 0 & 0 \\ 0 & 0 & 0 & -\frac{1}{\rho} & 0 & 0 & 0 & 0 & 0 \\ 0 & 0 & 0 & 0 & 0 & -\frac{1}{\rho} & 0 & 0 & 0 \end{pmatrix}, \quad (5)$$

$$B_{pq} = \begin{pmatrix} 0 & 0 & 0 & 0 & 0 & 0 & -c_{16} & -c_{12} & -c_{14} \\ 0 & 0 & 0 & 0 & 0 & 0 & -c_{26} & -c_{22} & -c_{24} \\ 0 & 0 & 0 & 0 & 0 & 0 & -c_{36} & -c_{23} & -c_{34} \\ 0 & 0 & 0 & 0 & 0 & 0 & -c_{66} & -c_{26} & -c_{46} \\ 0 & 0 & 0 & 0 & 0 & 0 & -c_{46} & -c_{24} & -c_{44} \\ 0 & 0 & 0 & 0 & 0 & 0 & -c_{56} & -c_{25} & -c_{45} \\ 0 & 0 & 0 & -\frac{1}{\rho} & 0 & 0 & 0 & 0 & 0 \\ 0 & -\frac{1}{\rho} & 0 & 0 & 0 & 0 & 0 & 0 & 0 \\ 0 & 0 & 0 & 0 & -\frac{1}{\rho} & 0 & 0 & 0 & 0 \end{pmatrix}, \quad (6)$$

$$C_{pq} = \begin{pmatrix} 0 & 0 & 0 & 0 & 0 & 0 & -c_{15} & -c_{14} & -c_{13} \\ 0 & 0 & 0 & 0 & 0 & 0 & -c_{25} & -c_{24} & -c_{23} \\ 0 & 0 & 0 & 0 & 0 & 0 & -c_{35} & -c_{34} & -c_{33} \\ 0 & 0 & 0 & 0 & 0 & 0 & -c_{56} & -c_{46} & -c_{36} \\ 0 & 0 & 0 & 0 & 0 & 0 & -c_{45} & -c_{44} & -c_{34} \\ 0 & 0 & 0 & 0 & 0 & 0 & -c_{55} & -c_{45} & -c_{35} \\ 0 & 0 & 0 & 0 & 0 & -\frac{1}{\rho} & 0 & 0 & 0 \\ 0 & 0 & 0 & 0 & -\frac{1}{\rho} & 0 & 0 & 0 & 0 \\ 0 & 0 & -\frac{1}{\rho} & 0 & 0 & 0 & 0 & 0 & 0 \end{pmatrix}, \quad (7)$$

where the coefficients c_{ij} are those of the anisotropic elastic matrix M_{ij} of (2) or (3) and ρ is the mass density of the material. We remark that analytically determining the eigenstructure the Jacobian matrices defined in (5), (6) and (7) is much more difficult for the anisotropic case than for the purely isotropic case as presented in the previous work (Dumbser & Käser 2006; Käser, Dumbser, de la Puente & Igel 2006). As shown in the following Section 3 this leads to modifications in the formulation of the ADER-DG scheme.

3 THE NUMERICAL SCHEME

The computational domain $\Omega \in \mathbb{R}^3$ is divided into conforming tetrahedral elements $\mathcal{T}^{(m)}$ being addressed by a unique index (m). Furthermore, we suppose the matrices A_{pq} , B_{pq} , and C_{pq} to be piecewise constant inside an element $\mathcal{T}^{(m)}$. The numerical solution Q_h of equation (4) is approximated as shown in (Dumbser & Käser 2006) inside each tetrahedron $\mathcal{T}^{(m)}$ by a linear combination of space-dependent but

time-independent polynomial basis functions $\Phi_l(\xi, \eta, \zeta)$ of degree N with support $\mathcal{T}^{(m)}$ and with only time-dependent degrees of freedom $\hat{Q}_{pl}^{(m)}(t)$, i.e.

$$\left(Q_h^{(m)}\right)_p(\xi, \eta, \zeta, t) = \hat{Q}_{pl}^{(m)}(t)\Phi_l(\xi, \eta, \zeta), \quad (8)$$

where ξ, η and ζ are the coordinates in a canonical reference element \mathcal{T}_E . For a detailed definition of these coordinates together with the basis functions Φ_l see (Dumbser & Käser 2006; Dumbser, Käser & de la Puente 2006). Multiplying (4) by the test function Φ_k and integrating over a tetrahedral element $\mathcal{T}^{(m)}$ gives

$$\int_{\mathcal{T}^{(m)}} \Phi_k \frac{\partial Q_p}{\partial t} dV + \int_{\mathcal{T}^{(m)}} \Phi_k \left(A_{pq} \frac{\partial Q_q}{\partial x} + B_{pq} \frac{\partial Q_q}{\partial y} + C_{pq} \frac{\partial Q_q}{\partial z} \right) dV = 0. \quad (9)$$

By applying integration by parts to the last integral of (9) we obtain

$$\int_{\mathcal{T}^{(m)}} \Phi_k \frac{\partial Q_p}{\partial t} dV + \int_{\partial\mathcal{T}^{(m)}} \Phi_k F_p^h dS - \int_{\mathcal{T}^{(m)}} \left(\frac{\partial \Phi_k}{\partial x} A_{pq} Q_q + \frac{\partial \Phi_k}{\partial y} B_{pq} Q_q + \frac{\partial \Phi_k}{\partial z} C_{pq} Q_q \right) dV = 0, \quad (10)$$

where a numerical flux F_p^h has been introduced in the surface integral since Q_h may be discontinuous at an element boundary. Here, two major changes with respect to the isotropic case appear.

First, we need to introduce the matrix $\tilde{A}^{(m)}$ which is similar to the matrix A of (5), however, with the entries c_{ij} rotated from the global coordinate system to a local coordinate system of a tetrahedron's face. This local coordinate system is defined by the normal vector $\vec{n} = (n_x, n_y, n_z)^T$ and the two tangential vectors $\vec{s} = (s_x, s_y, s_z)^T$ and $\vec{t} = (t_x, t_y, t_z)^T$, which lie in the plane determined by the face of the tetrahedron and are orthogonal to each other and to the normal vector \vec{n} . Usually we define vector \vec{s} such that it points from the local face node 1 to the local face node 2. The exact definitions of the vectors \vec{n} , \vec{s} and \vec{t} as well as the local vertex numbering of a tetrahedral element can be found in (Dumbser & Käser 2006). The rotation to this local coordinate system is done by applying the so-called Bond's matrix \mathcal{N} (Bond 1976; Okaya & McEvelly 2003)

$$\mathcal{N} = \begin{pmatrix} n_x^2 & n_y^2 & n_z^2 & 2n_z n_y & 2n_z n_x & 2n_y n_x \\ s_x^2 & s_y^2 & s_z^2 & 2s_z s_y & 2s_z s_x & 2s_y s_x \\ t_x^2 & t_y^2 & t_z^2 & 2t_z t_y & 2t_z t_x & 2t_y t_x \\ s_x t_x & s_y t_y & s_z t_z & s_y t_z + s_z t_y & s_x t_z + s_z t_x & s_y t_x + s_x t_y \\ t_x n_x & t_y n_y & t_z n_z & n_y t_z + n_z t_y & n_x t_z + n_z t_x & n_y t_x + n_x t_y \\ n_x s_x & n_y s_y & n_z s_z & n_y s_z + s_z n_y & n_x s_z + n_z s_x & n_y s_x + n_x s_y \end{pmatrix} \quad (11)$$

to the Hooke's matrix \mathcal{C} of the global reference system

$$\mathcal{C} = \begin{pmatrix} c_{11} & c_{12} & c_{13} & c_{14} & c_{15} & c_{16} \\ c_{12} & c_{22} & c_{23} & c_{24} & c_{25} & c_{26} \\ c_{13} & c_{23} & c_{33} & c_{34} & c_{35} & c_{36} \\ c_{14} & c_{24} & c_{34} & c_{44} & c_{45} & c_{46} \\ c_{15} & c_{25} & c_{35} & c_{45} & c_{55} & c_{56} \\ c_{16} & c_{26} & c_{36} & c_{46} & c_{56} & c_{66} \end{pmatrix} \quad (12)$$

leading to the Hooke's matrix $\tilde{\mathcal{C}}$ in the local reference system of the tetrahedron's boundary face

$$\tilde{\mathcal{C}} = \mathcal{N} \cdot \mathcal{C} \cdot \mathcal{N}^T. \quad (13)$$

We remark that in the isotropic case matrix \mathcal{C} is invariant under coordinate transformation, i.e. $\tilde{\mathcal{C}}_{iso} = \mathcal{C}_{iso}$. Therefore, this rotation could be skipped for the isotropic case discussed in (Dumbser & Käser 2006; Käser, Dumbser, de la Puente & Igel 2006).

The second modification comes through the different approaches for the numerical flux computation. The general definition of the our numerical flux incorporating anisotropic material can be written as

$$F_p^h = \frac{1}{2} \left(T_{pq} \tilde{A}_{qr}^{(m)} (T_{rs})^{-1} + \Theta_{ps} \right) \hat{Q}_{sl}^{(m)} \phi_l^{(m)} + \frac{1}{2} \left(T_{pq} \tilde{A}_{qr}^{(m)} (T_{rs})^{-1} - \Theta_{ps} \right) \hat{Q}_{sl}^{(m_j)} \phi_l^{(m_j)}, \quad (14)$$

where $\hat{Q}^{(m)} \phi^{(m)}$ and $\hat{Q}^{(m_j)} \phi^{(m_j)}$ are the boundary extrapolated values of the numerical solution from element $\mathcal{T}^{(m)}$ and its j -th side neighbour $\mathcal{T}^{(m_j)}$, respectively. To simplify notation, in the following, we drop the index j indicating the j -th face of the tetrahedron $\mathcal{T}^{(m)}$. The $\tilde{A}_{qr}^{(m)}$ is the Jacobian matrix A_{pq} defined in (5) but with the rotated coefficients c_{ij} from the Hooke's matrix $\tilde{\mathcal{C}}$ as computed in (13). The rotation matrix T_{pq} that transforms all variables of Q_p from (4) into the reference system associated to the tetrahedron's j -th face has the

same expression as in the isotropic case in (Dumbser & Käser 2006) and reads as

$$T_{pq} = \begin{pmatrix} n_x^2 & s_x^2 & t_x^2 & 2n_x s_x & 2s_x t_x & 2n_x t_x & 0 & 0 & 0 \\ n_y^2 & s_y^2 & t_y^2 & 2n_y s_y & 2s_y t_y & 2n_y t_y & 0 & 0 & 0 \\ n_z^2 & s_z^2 & t_z^2 & 2n_z s_z & 2s_z t_z & 2n_z t_z & 0 & 0 & 0 \\ n_y n_x & s_y s_x & t_y t_x & n_y s_x + n_x s_y & s_y t_x + s_x t_y & n_y t_x + n_x t_y & 0 & 0 & 0 \\ n_z n_y & s_z s_y & t_z t_y & n_z s_y + n_y s_z & s_z t_y + s_y t_z & n_z t_y + n_y t_z & 0 & 0 & 0 \\ n_z n_x & s_z s_x & t_z t_x & n_z s_x + n_x s_z & s_z t_x + s_x t_z & n_z t_x + n_x t_z & 0 & 0 & 0 \\ 0 & 0 & 0 & 0 & 0 & 0 & n_x & s_x & t_x \\ 0 & 0 & 0 & 0 & 0 & 0 & n_y & s_y & t_y \\ 0 & 0 & 0 & 0 & 0 & 0 & n_z & s_z & t_z \end{pmatrix}. \quad (15)$$

The matrix Θ_{ps} is a numerical viscosity term whose particular form determines the flux type we wish to use and depends on the orientation of the interface with the j -th side neighbour. In the following, we introduce the Godunov flux and the Rusanov flux which have a numerical viscosity matrix of the form

$$(\Theta_{ps})_{Rusanov} = \alpha_{max} I_{ps}, \quad (16)$$

$$(\Theta_{ps})_{Godunov} = T_{pq} \left| \tilde{A}_{qr} \right| T_{rs}, \quad (17)$$

where I_{ps} is the identity matrix. The computation of the Godunov flux requires knowledge of the eigenstructure of the Jacobian matrix \tilde{A}_{qr} . This, for the anisotropic case, is a non-trivial issue as it requires the computation of $\left| \tilde{A}_{qr} \right|$, which in turn usually requires the knowledge of the left and right eigenvectors of \tilde{A}_{qr} . A new method to obtain the Godunov flux in (17) for anisotropic material is presented in the Appendix A. Alternatively, the Rusanov flux (LeVeque 2002) requires only the knowledge of the maximum eigenvalue of \tilde{A}_{qr} . This value is $\alpha_{max} = \max(\alpha_i)$, where α_i are the roots of the following polynomial of α

$$XYZ - Xc_{56}^2 - Yc_{15}^2 - Zc_{16}^2 + 2c_{15}c_{16}c_{56} = 0, \quad (18)$$

where the coefficients c_{ij} are the entries of the Hooke's matrix \tilde{C} of (13) rotated into the local reference system of the j -th side of the tetrahedral element. Furthermore, we used the substitutions $X = c_{11} - \alpha^2 \rho$, $Y = c_{66} - \alpha^2 \rho$ and $Z = c_{55} - \alpha^2 \rho$. As can be seen from (18) we are searching the maximum value of the possibly 6 roots of polynomial of degree 6. However, the substitutions using X , Y and Z tell us, that there are only three different values to search for, as (18) represents a cubic polynomial of α^2 . We can exclude the possibility of having complex eigenvalues, i.e. $\alpha^2 < 0$, as this would imply the loss of hyperbolicity of the PDE system in (4). The physical interpretation of the eigenvalues is that they represent the speed at which the different wave types are propagating in normal direction through the j -th element face. This is a known result for the anisotropic phase wave speeds (Crampin 1981) which appears here naturally from the eigendecomposition of the jacobians of our scheme (5). In general the resulting waves are called *quasi-waves* qP , qS_1 and qS_2 ; ordered in decreasing magnitude of their velocities (Crampin 1981). For the isotropic case we would get the positive and negative P-wave velocity and two positive and negative S-wave velocity of the same absolute value. These values correspond to the two differently and perpendicularly to each other polarized S-waves.

Once the maximum eigenvalue α_{max} is determined, the Rusanov flux is given via (16). As the full derivation of the numerical scheme would go beyond the scope of this work we refer the reader to previous work (Käser & Dumbser 2006; Dumbser & Käser 2006) for the mathematical details. Instead we give the final form of the fully discrete ADER-DG scheme, which after transformation into the canonical reference element \mathcal{T}_E and time integration over one time step Δt from time level n to the following time level $n + 1$ reads as

$$\begin{aligned} & \left[\left(\hat{Q}_{pl}^{(m)} \right)^{n+1} - \left(\hat{Q}_{pl}^{(m)} \right)^n \right] |J| M_{kl} + \\ & + \frac{1}{2} \sum_{j=1}^4 \left(T_{pq}^j \tilde{A}_{qr}^{(m)} (T_{rs}^j)^{-1} + \Theta_{ps}^j \right) |S_j| F_{kl}^{-,j} \cdot I_{qlmn}(\Delta t) \left(\hat{Q}_{mn}^{(m)} \right)^n + \\ & + \frac{1}{2} \sum_{j=1}^4 \left(T_{pq}^j \tilde{A}_{qr}^{(m)} (T_{rs}^j)^{-1} - \Theta_{ps}^j \right) |S_j| F_{kl}^{+,j,i,h} \cdot I_{qlmn}(\Delta t) \left(\hat{Q}_{mn}^{(m_j)} \right)^n - \\ & - A_{pq}^* |J| K_{kl}^\xi \cdot I_{qlmn}(\Delta t) \left(\hat{Q}_{mn}^{(m)} \right)^n - B_{pq}^* |J| K_{kl}^\eta \cdot I_{qlmn}(\Delta t) \left(\hat{Q}_{mn}^{(m)} \right)^n - C_{pq}^* |J| K_{kl}^\zeta \cdot I_{qlmn}(\Delta t) \left(\hat{Q}_{mn}^{(m)} \right)^n = 0, \end{aligned} \quad (19)$$

where $I_{plqm}(\Delta t)$ represents the high order ADER time integration operator that is applied to the degrees of freedom $\left(\hat{Q}_{mn}^{(m)} \right)^n$ at time level n . The matrices M_{kl} , $F_{kl}^{-,j}$ and K_{kl} are the mass matrix, flux and stiffness matrices, respectively, include space integrations of our basis functions and can be computed beforehand as shown in more detail in (Dumbser & Käser 2006). The resulting ADER-DG scheme provides automatically high order approximation in space and time and allows us to update the values of our unknown variables from a timestep t^n to a following t^{n+1} without store any intermediate values as typically necessary for classical multi-stage Runge-Kutta time stepping schemes.

Furthermore, the scheme has a very local character, as the evolution of the variables in time within the element $\mathcal{T}^{(m)}$ depends only on the variables associated to the element $\mathcal{T}^{(m)}$ itself and its direct neighbours $\mathcal{T}^{(m_j)}$, with $j = 1, \dots, 4$.

4 COUPLING OF ANISOTROPY AND VISCOELASTICITY

Anisotropy and viscoelastic attenuation play an important role as secondary effects in seismic wave propagation modeling. The incorporation of anisotropy into the ADER-DG framework has been discussed in the previous Sections 2 and 3. Viscoelastic attenuation, however, was introduced in (Käser, Dumbser, de la Puente & Igel 2006). In order to accurately couple both effects we use the concepts of mean and deviatoric stresses first presented in (Carcione 1995) and adapt them to the rheological model of the Generalized Maxwell Body (GMB) as suggested in (Emmerich & Korn 1987). At first we define the underlying physical theory of viscoelastic anisotropy. Then we present in detail how viscoelasticity changes the anisotropic PDE system as given in (4). Finally, we explain how the ADER-DG scheme presented in Section 3 has to be modified in order to couple anisotropy and viscoelasticity.

4.1 Viscoelastic Anisotropic Wave Propagation

The mean stress $\bar{\sigma}$ and mean strain $\bar{\varepsilon}$, as well as the deviatoric stress $\bar{\sigma}^D$ and deviatoric strain $\bar{\varepsilon}^D$ are defined as

$$\bar{\sigma} \equiv \frac{1}{3}(\sigma_{xx} + \sigma_{yy} + \sigma_{zz}), \quad (20)$$

$$\bar{\varepsilon} \equiv \frac{1}{3}(\varepsilon_{xx} + \varepsilon_{yy} + \varepsilon_{zz}), \quad (21)$$

$$\bar{\sigma}^D \equiv \bar{\sigma} - \bar{\sigma}, \quad (22)$$

$$\bar{\varepsilon}^D \equiv \bar{\varepsilon} - \bar{\varepsilon}, \quad (23)$$

where we remark that the mean stress and strain are invariant under coordinate transformation. As shown in (Carcione 2002) we need a total of four attenuation moduli to model viscoelastic attenuation in an anisotropic medium. One purely dilatational modulus and three shear moduli. In this case, the mean stress $\bar{\sigma}$ depends only on the dilatational modulus while the deviatoric stress $\bar{\sigma}^D$ only depends on the shear moduli. The stress-strain relation in the general case can be expressed in the frequency domain or in the time domain, e.g. see (Moczo, Kristek & Halada 2004) for the isotropic case, which reads in the anisotropic case (Carcione 1995) as

$$\bar{\sigma}_i(\omega) = M_{ij}(\omega)\bar{\varepsilon}_j(\omega), \quad (24)$$

$$\bar{\sigma}_i(t) = \frac{\partial}{\partial t}(\Psi_{ij}(t)) * \bar{\varepsilon}_j(t) = M_{ij}(t) * \bar{\varepsilon}_j(t), \quad (25)$$

where the so-called *relaxation matrix* $\Psi_{ij}(t)$ is given by

$$\Psi_{ij}(t) = \begin{pmatrix} \Psi_{11}(t) & \Psi_{12}(t) & \Psi_{13}(t) & 2c_{14} & 2c_{15} & 2c_{16} \\ \Psi_{12}(t) & \Psi_{22}(t) & \Psi_{23}(t) & 2c_{24} & 2c_{25} & 2c_{26} \\ \Psi_{13}(t) & \Psi_{23}(t) & \Psi_{33}(t) & 2c_{34} & 2c_{35} & 2c_{36} \\ c_{14} & c_{24} & c_{34} & 2\Psi_{44}(t) & 2c_{45} & 2c_{46} \\ c_{15} & c_{25} & c_{35} & 2c_{45} & 2\Psi_{55}(t) & 2c_{56} \\ c_{16} & c_{26} & c_{36} & 2c_{46} & 2c_{56} & 2\Psi_{66}(t) \end{pmatrix} \cdot H(t). \quad (26)$$

Here, $H(t)$ is the Heaviside step function and the components $\Psi_{ij}(t)$ can be expressed as

$$\Psi_{ij}(t) = \sum_{k=0}^4 g_{ij}^{(k)} \chi^{(k)}(t) \quad \text{with} \quad g_{ij}^{(k)} \in \mathbb{R}, \quad (27)$$

where $g_{ij}^{(k)}$ are real numbers, combinations of the c_{ij} entries of the elastic Hooke's tensor and the $\chi^{(k)}$, called *relaxation functions*, contain the time functionality of the relaxation matrix's entries, normalized such that $\chi^{(k)} = 1$ for $t = 0$ and by defining the mode's complex modulus as $M^{(k)}(\omega) = d(\chi^{(k)}(t)H(t))/dt$, this modulus behaves as $M^{(k)}(\omega) \rightarrow 1$ for $\omega \rightarrow \infty$.

In (Moczo, Kristek & Halada 2004) we can find a formulation of the GMB relaxation mechanisms that, once normalized, can be used to express the $\chi^{(k)}(t)$ as

$$\begin{aligned} \chi^{(k)}(t) &= 1 - \sum_{\ell=1}^n Y_{\ell}^{(k)} (1 - e^{-\omega_{\ell} t}), & \text{for } k = 1, 2, 3, 4 \\ \chi^{(k)}(t) &= 1, & \text{for } k = 0 \end{aligned} \quad (28)$$

where n is the number of attenuating mechanisms used. These GMB relaxation functions fulfill the conditions discussed above. The $k = 0$ case is shown for completion but doesn't represent a relaxation function but, more accurately, a lack of it. As we have a constant $\chi^{(0)}$ value we obtain an instantaneous response, so that we are talking about an elastic mode. We remark that in the elastic case all $g_{ij}^{(k)} = 0$, if $k \neq 0$, thus having exclusively that instantaneous response and, as a consequence, no energy losses. In the viscoelastic isotropic case we have $g_{ij}^{(k)} = 0$,

except for $k = 0$, $k = 1$ (dilatational mode) and $k = 2$ (first shear mode).

Finally we can find the coefficients $g_{ij}^{(k)}$ that ensure the separation of the dilatational and shear modes of the attenuation (Carcione 2002) giving us the entries of (27) by

$$\begin{aligned}
 \Psi_{ii}(t) &= c_{ii} - (\bar{\lambda} + 2\bar{\mu}) + (\bar{\lambda} + \frac{4}{3}\bar{\mu})\chi^{(1)}(t) + (\frac{2}{3}\bar{\mu})\chi^{(2)}(t), & \text{for } i \leq 3 \\
 \Psi_{ij}(t) &= c_{ij} - \bar{\lambda} + (\bar{\lambda} + \frac{2}{3}\bar{\mu})\chi^{(1)}(t) - \frac{2}{3}\bar{\mu}\chi^{(2)}(t), & \text{for } i, j \leq 3 \text{ and } i \neq j \\
 \Psi_{44}(t) &= c_{44}\chi^{(2)}(t) \\
 \Psi_{55}(t) &= c_{55}\chi^{(3)}(t) \\
 \Psi_{66}(t) &= c_{66}\chi^{(4)}(t)
 \end{aligned} \tag{29}$$

with the definitions $\bar{\mu} \equiv \frac{1}{3}(c_{44} + c_{55} + c_{66})$ and $\bar{\lambda} \equiv \frac{1}{3}(c_{11} + c_{22} + c_{33}) - 2\bar{\mu}$. We can also redefine the anelastic coefficients such as $\bar{\lambda}Y_\ell^\lambda = (\bar{\lambda} + \frac{2}{3}\bar{\mu})Y_\ell^{(1)} - \frac{2}{3}\bar{\mu}Y_\ell^{(2)}$, $Y_\ell^{\mu_1} = Y_\ell^{(2)}$, $Y_\ell^{\mu_2} = Y_\ell^{(3)}$ and $Y_\ell^{\mu_3} = Y_\ell^{(4)}$.

Now, making use of the last identity in (25) we derivate in time the components of the tensor $\Psi_{ij}(t)$ that are given in (29) to obtain the anisotropic viscoelastic stress-strain relation

$$\begin{pmatrix} \sigma_{xx} \\ \sigma_{yy} \\ \sigma_{zz} \\ \sigma_{yz} \\ \sigma_{xz} \\ \sigma_{xy} \end{pmatrix} = \begin{pmatrix} c_{11} & c_{12} & c_{13} & 2c_{14} & 2c_{15} & 2c_{16} \\ c_{12} & c_{22} & c_{23} & 2c_{24} & 2c_{25} & 2c_{26} \\ c_{13} & c_{23} & c_{33} & 2c_{34} & 2c_{35} & 2c_{36} \\ c_{14} & c_{24} & c_{34} & 2c_{44} & 2c_{45} & 2c_{46} \\ c_{15} & c_{25} & c_{35} & 2c_{45} & 2c_{55} & 2c_{56} \\ c_{16} & c_{26} & c_{36} & 2c_{46} & 2c_{56} & 2c_{66} \end{pmatrix} \begin{pmatrix} \varepsilon_{xx} \\ \varepsilon_{yy} \\ \varepsilon_{zz} \\ \varepsilon_{yz} \\ \varepsilon_{xz} \\ \varepsilon_{xy} \end{pmatrix} - \sum_{\ell=1}^n \begin{pmatrix} \bar{\lambda}Y_\ell^\lambda + 2\bar{\mu}Y_\ell^{\mu_1} & \bar{\lambda}Y_\ell^\lambda & \bar{\lambda}Y_\ell^\lambda & 0 & 0 & 0 \\ \bar{\lambda}Y_\ell^\lambda & \bar{\lambda}Y_\ell^\lambda + 2\bar{\mu}Y_\ell^{\mu_1} & \lambda Y_\ell^\lambda & 0 & 0 & 0 \\ \bar{\lambda}Y_\ell^\lambda & \bar{\lambda}Y_\ell^\lambda & \bar{\lambda}Y_\ell^\lambda + 2\bar{\mu}Y_\ell^{\mu_1} & 0 & 0 & 0 \\ 0 & 0 & 0 & 2c_{44}Y_\ell^{\mu_1} & 0 & 0 \\ 0 & 0 & 0 & 0 & 2c_{55}Y_\ell^{\mu_2} & 0 \\ 0 & 0 & 0 & 0 & 0 & 2c_{66}Y_\ell^{\mu_3} \end{pmatrix} \begin{pmatrix} \vartheta_{xx}^\ell \\ \vartheta_{yy}^\ell \\ \vartheta_{zz}^\ell \\ \vartheta_{yz}^\ell \\ \vartheta_{xz}^\ell \\ \vartheta_{xy}^\ell \end{pmatrix}. \tag{30}$$

Here, the the anelastic functions $\vec{\vartheta}^\ell = (\vartheta_{xx}^\ell, \vartheta_{yy}^\ell, \vartheta_{zz}^\ell, \vartheta_{yz}^\ell, \vartheta_{xz}^\ell, \vartheta_{xy}^\ell)^T$ are defined by

$$\vartheta_j^\ell(t) = \omega_\ell \frac{\partial}{\partial t} \left(\int_{-\infty}^t \varepsilon_j(\tau) e^{-\omega_\ell(t-\tau)} d\tau \right), \tag{31}$$

as shown in (Moczo, Kristek & Halada 2004). The anelastic coefficients have to be fitted to the particular Q -law over a desired frequency range by using a number of relaxation frequencies ω_ℓ as outlined in more detail in (Käser, Dumbser, de la Puente & Igel 2006).

Notice here that this formulation even admits anisotropic attenuation, meaning that we can have different Q values for each of the 3 shear attenuating modes. However, our knowledge of the quality factors Q inside the earth is often poor and rarely would allow us to consider any dependence on direction of the values of the Q -factors. Therefore, in the following we limit ourselves to the case in which attenuation is considered as an isotropic effect, even if the medium is anisotropic. This means, that $Q^{\mu_1} = Q^{\mu_2} = Q^{\mu_3}$ and therefore we can define $Y_\ell^\mu \equiv Y_\ell^{\mu_1} = Y_\ell^{\mu_2} = Y_\ell^{\mu_3}$. Note, that the stress-strain relation in (30) provides the general case from which we can infer the anisotropic elastic case by defining $Y_\ell^\lambda = 0$ and $Y_\ell^{\mu_i} = 0$, thus recovering (3). The viscoelastic isotropic case is obtained by defining $c_{11} = c_{22} = c_{33} = \lambda + 2\mu$, $c_{12} = c_{13} = c_{23} = \lambda$ and $c_{44} = c_{55} = c_{66} = \mu$ with all other coefficients c_{ij} equal to zero. This way, we also obtain $\bar{\lambda} = \lambda$ and $\bar{\mu} = \mu$ as a consequence.

The use of the anelastic functions ϑ_j requires the storage of 6 new variables per attenuation mechanism in each tetrahedral element that have to be updated at every time step, as already shown in (Käser, Dumbser, de la Puente & Igel 2006) for the anelastic case. This is done by solving an additional set of $6n$ linear partial differential equations given by

$$\frac{\partial}{\partial t} \vartheta_j^\ell(t) + \omega_\ell \vartheta_j^\ell(t) = \omega_\ell \frac{\partial}{\partial t} \varepsilon_j(t), \tag{32}$$

where $\ell = 1, \dots, n$ is the index of the attenuation mechanism. The total number of attenuation mechanisms is n and $j = 1, \dots, 6$ for the 6 stress components in (30). A detailed description of the resulting coupled linear system of equations is given in the following Section 4.2.

4.2 The Coupled Equation System

As shown in (Käser, Dumbser, de la Puente & Igel 2006), the new enlarged system of $n_v = 9 + 6n$ partial differential equations including 9 elastic and $6n$ anelastic variables can be written in the compact form

$$\frac{\partial Q_p}{\partial t} + \check{A}_{pq} \frac{\partial Q_q}{\partial x} + \check{B}_{pq} \frac{\partial Q_q}{\partial y} + \check{C}_{pq} \frac{\partial Q_q}{\partial z} = \check{E}_{pq} Q_q, \quad (33)$$

where E denotes the so-called *reaction term* and takes into account the energy losses introduced by the viscoelastic medium. Note that the dimensions of the variable vector Q , the Jacobian matrices \check{A} , \check{B} , \check{C} and the source matrix \check{E} now depend on the number n of attenuation mechanisms. To keep the notation as simple as possible and without loss of generality, in the following we assume that the order of the equations in (33) is such, that $p, q \in [1, \dots, 9]$ denote the elastic part and $p, q \in [10, \dots, n_v]$, denote the anelastic part of the system, represented by the variables in (31) and the corresponding equations in (32).

As the Jacobian matrices \check{A} , \check{B} and \check{C} as well as the source matrix \check{E} are sparse and show some particular symmetry pattern and as their dimensions may become impractical for notation, we will use the block-matrix syntax.

Therefore, we decompose the Jacobian matrices as follows:

$$\check{A} = \begin{bmatrix} A & 0 \\ A_a & 0 \end{bmatrix} \in \mathbb{R}^{n_v \times n_v}, \quad \check{B} = \begin{bmatrix} B & 0 \\ B_a & 0 \end{bmatrix} \in \mathbb{R}^{n_v \times n_v}, \quad \check{C} = \begin{bmatrix} C & 0 \\ C_a & 0 \end{bmatrix} \in \mathbb{R}^{n_v \times n_v}, \quad (34)$$

where $A, B, C \in \mathbb{R}^{9 \times 9}$ are the Jacobians of the purely anisotropic elastic part as given in (5)- (7). The matrices A_a, B_a, C_a include the anelastic part and exhibit themselves a block structure of the form:

$$A_a = \begin{bmatrix} A_1 \\ \vdots \\ A_n \end{bmatrix} \in \mathbb{R}^{6n \times 9}, \quad B_a = \begin{bmatrix} B_1 \\ \vdots \\ B_n \end{bmatrix} \in \mathbb{R}^{6n \times 9}, \quad C_a = \begin{bmatrix} C_1 \\ \vdots \\ C_n \end{bmatrix} \in \mathbb{R}^{6n \times 9}, \quad (35)$$

where each sub-matrix $A_\ell, B_\ell, C_\ell \in \mathbb{R}^{6 \times 9}$, with $\ell = 1, \dots, n$, contains the relaxation frequency ω_ℓ of the ℓ -th attenuation mechanism in the form:

$$A_\ell = \omega_\ell \cdot \begin{pmatrix} 0 & 0 & 0 & 0 & 0 & 0 & -1 & 0 & 0 \\ 0 & 0 & 0 & 0 & 0 & 0 & 0 & 0 & 0 \\ 0 & 0 & 0 & 0 & 0 & 0 & 0 & 0 & 0 \\ 0 & 0 & 0 & 0 & 0 & 0 & 0 & -\frac{1}{2} & 0 \\ 0 & 0 & 0 & 0 & 0 & 0 & 0 & 0 & 0 \\ 0 & 0 & 0 & 0 & 0 & 0 & 0 & 0 & -\frac{1}{2} \end{pmatrix}, \quad (36)$$

$$B_\ell = \omega_\ell \cdot \begin{pmatrix} 0 & 0 & 0 & 0 & 0 & 0 & 0 & 0 & 0 \\ 0 & 0 & 0 & 0 & 0 & 0 & 0 & -1 & 0 \\ 0 & 0 & 0 & 0 & 0 & 0 & 0 & 0 & 0 \\ 0 & 0 & 0 & 0 & 0 & 0 & -\frac{1}{2} & 0 & 0 \\ 0 & 0 & 0 & 0 & 0 & 0 & 0 & 0 & -\frac{1}{2} \\ 0 & 0 & 0 & 0 & 0 & 0 & 0 & 0 & 0 \end{pmatrix}, \quad (37)$$

$$C_\ell = \omega_\ell \cdot \begin{pmatrix} 0 & 0 & 0 & 0 & 0 & 0 & 0 & 0 & 0 \\ 0 & 0 & 0 & 0 & 0 & 0 & 0 & 0 & 0 \\ 0 & 0 & 0 & 0 & 0 & 0 & 0 & 0 & -1 \\ 0 & 0 & 0 & 0 & 0 & 0 & 0 & 0 & 0 \\ 0 & 0 & 0 & 0 & 0 & 0 & 0 & -\frac{1}{2} & 0 \\ 0 & 0 & 0 & 0 & 0 & 0 & -\frac{1}{2} & 0 & 0 \end{pmatrix}. \quad (38)$$

The matrix \check{E} in (4) representing the reactive source term that couples the anelastic functions to the original elastic system can be decomposed as

$$\check{E} = \begin{bmatrix} 0 & E \\ 0 & E' \end{bmatrix} \in \mathbb{R}^{n_v \times n_v}, \quad (39)$$

with E exhibiting the block structure

$$E = [E_1, \dots, E_n] \in \mathbb{R}^{9 \times 6n}. \quad (40)$$

Here, each matrix $E_\ell \in \mathbb{R}^{9 \times 6}$, with $\ell = 1, \dots, n$, contains the anelastic coefficients Y_ℓ^λ and Y_ℓ^μ of the ℓ -th mechanism in the form:

$$E_\ell = \begin{pmatrix} \bar{\lambda}Y_\ell^\lambda + 2\bar{\mu}Y_\ell^\mu & \bar{\lambda}Y_\ell^\lambda & \bar{\lambda}Y_\ell^\lambda & 0 & 0 & 0 \\ \bar{\lambda}Y_\ell^\lambda & \bar{\lambda}Y_\ell^\lambda + 2\bar{\mu}Y_\ell^\mu & \lambda Y_\ell^\lambda & 0 & 0 & 0 \\ \bar{\lambda}Y_\ell^\lambda & \bar{\lambda}Y_\ell^\lambda & \bar{\lambda}Y_\ell^\lambda + 2\bar{\mu}Y_\ell^\mu & 0 & 0 & 0 \\ 0 & 0 & 0 & 2c_{66}Y_\ell^\mu & 0 & 0 \\ 0 & 0 & 0 & 0 & 2c_{44}Y_\ell^\mu & 0 \\ 0 & 0 & 0 & 0 & 0 & 2c_{55}Y_\ell^\mu \\ 0 & 0 & 0 & 0 & 0 & 0 \\ 0 & 0 & 0 & 0 & 0 & 0 \\ 0 & 0 & 0 & 0 & 0 & 0 \end{pmatrix}, \quad (41)$$

where we should notice the different ordering of the entries with respect to what we introduced in (30) as a consequence of the different order of the anelastic variables inside the variable vector Q . The matrix E' in (39) is a diagonal matrix and has the structure

$$E' = \begin{bmatrix} E'_1 & & 0 \\ & \ddots & \\ 0 & & E'_n \end{bmatrix} \in \mathbb{R}^{6n \times 6n}, \quad (42)$$

where each matrix $E'_\ell \in \mathbb{R}^{6 \times 6}$, with $\ell = 1, \dots, n$, is itself a diagonal matrix containing only the relaxation frequency ω_ℓ of the ℓ -th mechanism on its diagonal, i.e. $E'_\ell = -\omega_\ell \cdot I$ with $I \in \mathbb{R}^{6 \times 6}$ denoting the identity matrix.

As shown in the following Section 4.3, we can formulate the fully discrete ADER-DG scheme with conceptually only minor changes in order to obtain a high order numerical scheme for solving this new enlarged system of equations, that includes viscoelastic attenuation as well as the most general triclinic anisotropy.

4.3 The Coupled Numerical Scheme

As shown in more detail in (Käser, Dumbser, de la Puente & Igel 2006) the numerical scheme including viscoelastic attenuation changes due to the enlargement of the PDE system and the addition of the reaction term E . Therefore, the discrete formulation of the ADER-DG scheme for anisotropic elastic media as given in (19) is now written as

$$\begin{aligned} & \left[\left(\hat{Q}_{pl}^{(m)} \right)^{n+1} - \left(\hat{Q}_{pl}^{(m)} \right)^n \right] |J| M_{kl} + \\ & + \frac{1}{2} \sum_{j=1}^4 \left(\tilde{T}_{pr}^j \tilde{A}_{rs}^{(m)} (\tilde{T}_{sq}^j)^{-1} + \Theta_{pq}^{j,(m)} \right) |S_j| F_{kl}^{-,j} \cdot I_{qlmn}(\Delta t) \left(\hat{Q}_{mn}^{(m)} \right)^n + \\ & + \frac{1}{2} \sum_{j=1}^4 \left(\tilde{T}_{pr}^j \tilde{A}_{rs}^{(m)} (\tilde{T}_{sq}^j)^{-1} - \Theta_{pq}^{j,(m)} \right) |S_j| F_{kl}^{+,j,i,h} \cdot I_{qlmn}(\Delta t) \left(\hat{Q}_{mn}^{(m_j)} \right)^n - \\ & - \tilde{A}_{pq}^* |J| K_{kl}^\xi \cdot I_{qlmn}(\Delta t) \left(\hat{Q}_{mn}^{(m)} \right)^n - \tilde{B}_{pq}^* |J| K_{kl}^\eta \cdot I_{qlmn}(\Delta t) \left(\hat{Q}_{mn}^{(m)} \right)^n - \tilde{C}_{pq}^* |J| K_{kl}^\zeta \cdot I_{qlmn}(\Delta t) \left(\hat{Q}_{mn}^{(m)} \right)^n = \\ & = |J| \tilde{E}_{pq} \cdot I_{qlmn}(\Delta t) \left(\hat{Q}_{mn}^{(m)} \right)^n M_{kl}, \end{aligned} \quad (43)$$

where Θ_{ps} is specified by the particular numerical flux in (16) or (17). The matrix $\tilde{A}_{rs}^{(m)}$ now represents the enlarged matrix in (34) with the entries of (5) which are rotated through the Bond's transformation (13) as discussed in Section 3. We remark that α_{max} remains the same in the viscoelastic case, as the enlargement of the Jacobian matrices introduces only new eigenvalues equal to zero. Further details on the calculation of the Godunov flux in (17) for the anelastic part of the coupled system can be found in the Appendix A.

Besides, the rotation matrix \tilde{T}_{pq} becomes larger and for the case of anelasticity in (43) has the form

$$\tilde{T} = \begin{bmatrix} T^t & 0 & 0 \\ 0 & T^v & 0 \\ 0 & 0 & T_a \end{bmatrix} \in \mathbb{R}^{n_v \times n_v}, \quad (44)$$

where $T^t \in \mathbb{R}^{6 \times 6}$ is the rotation matrix responsible for the stress tensor rotation as in the purely elastic part and is given as

$$T^t = \begin{pmatrix} n_x^2 & s_x^2 & t_x^2 & 2n_x s_x & 2s_x t_x & 2n_x t_x \\ n_y^2 & s_y^2 & t_y^2 & 2n_y s_y & 2s_y t_y & 2n_y t_y \\ n_z^2 & s_z^2 & t_z^2 & 2n_z s_z & 2s_z t_z & 2n_z t_z \\ n_y n_x & s_y s_x & t_y t_x & n_y s_x + n_x s_y & s_y t_x + s_x t_y & n_y t_x + n_x t_y \\ n_z n_y & s_z s_y & t_z t_y & n_z s_y + n_y s_z & s_z t_y + s_y t_z & n_z t_y + n_y t_z \\ n_z n_x & s_z s_x & t_z t_x & n_z s_x + n_x s_z & s_z t_x + s_x t_z & n_z t_x + n_x t_z \end{pmatrix}. \quad (45)$$

Table 1. Coefficients for the anisotropic, orthorhombic material given in $[N \cdot m^{-2}]$ as used in the convergence study. All other coefficients are zero. The material density ρ is given in $kg \cdot m^{-3}$.

ρ	c_{11}	c_{12}	c_{13}	c_{22}	c_{23}	c_{33}	c_{44}	c_{55}	c_{66}
1	192	66	60	160	56	272	60	62	49

The matrix $T^v \in \mathbb{R}^{3 \times 3}$ is the rotation matrix responsible for the velocity vector rotation as in the purely elastic part and is given as

$$T^v = \begin{pmatrix} n_x & s_x & t_x \\ n_y & s_y & t_y \\ n_z & s_z & t_z \end{pmatrix}. \quad (46)$$

The matrix T_a in (44) is a block diagonal matrix and has the structure

$$T_a = \begin{bmatrix} T^t & & 0 \\ & \ddots & \\ 0 & & T^t \end{bmatrix} \in \mathbb{R}^{6n \times 6n}, \quad (47)$$

where each of the n sub-matrices T^t is the tensor rotation matrix given in (45). A more detailed description of an efficient implementation of the ADER-DG method for the anelastic case the reader is referred to (Käser, Dumbser, de la Puente & Igel 2006).

5 CONVERGENCE STUDY

In this section we present a numerical convergence study of the proposed ADER-DG approach on tetrahedral meshes, in order to demonstrate its arbitrarily high order of convergence in the presence of anisotropic material. We show results from second to seventh order ADER-DG schemes denoted by ADER-DG $\mathcal{O}2$ to ADER-DG $\mathcal{O}7$ respectively. We remark that the same order for space and time accuracy is obtained automatically.

Similar to previous work (Käser & Dumbser 2006; Dumbser & Käser 2006; Käser, Dumbser, de la Puente & Igel 2006) we determine the convergence orders by solving the three-dimensional, anisotropic, seismic wave equations on the unit-cube as sketched in Figure 1, i.e. on a computational domain $\Omega = [-1, 1] \times [-1, 1] \times [-1, 1] \in \mathbb{R}^3$ with periodic boundary conditions.

The homogeneous anisotropic material parameters are given in Table 1 and represent an orthorhombic material, similar to olivine as given in (Browaeys & Chevrot 2004). The analytic solution to this problem can be formulated as

$$Q_p(x, y, z, t) = Q_p^0 \cdot e^{i \cdot (\omega t - k_x x - k_y y - k_z z)}, \quad p = 1, \dots, 9 \quad (48)$$

where Q_p^0 is the initial amplitude vector of the 9 components, ω are the wave frequencies to determine and k_x , k_y and k_z are the wave numbers in x , y and z -direction, respectively. To confirm that anisotropy is treated correctly, we superimpose three plane waves $Q_p^{(l)}$, $l = 1, \dots, 3$, of the form given in (48) travelling perpendicular to each other along the coordinate axes, i.e. we have the three wave number vectors

$$\vec{k}^{(1)} = (k_x^{(1)}, k_y^{(1)}, k_z^{(1)})^T = (\pi, 0, 0)^T, \quad (49)$$

$$\vec{k}^{(2)} = (k_x^{(2)}, k_y^{(2)}, k_z^{(2)})^T = (0, \pi, 0)^T, \quad (50)$$

$$\vec{k}^{(3)} = (k_x^{(3)}, k_y^{(3)}, k_z^{(3)})^T = (0, 0, \pi)^T. \quad (51)$$

leading to a periodic, sinusoidal waves in the unit-cube.

In the following, we briefly line out, how we determine the wave frequencies ω . With the assumption, that equation (48) is the analytic solution of the governing equation (4), we calculate the first time and space derivatives of equation (48) analytically and plug them into equation (4). From there, we can derive the eigenproblem

$$(\check{A}_{pq} k_x + \check{B}_{pq} k_y + \check{C}_{pq} k_z) \cdot Q_q^0 = \omega \cdot Q_q^0, \quad p, q = 1, \dots, 9. \quad (52)$$

Solving the three eigenproblem (52) for each wave l gives us the matrix $R_{pq}^{(l)}$ of right eigenvectors $R_{p1}^{(l)}, \dots, R_{p9}^{(l)}$ and the eigenvalues $\omega_p^{(l)}$ for each wave.

Recalling, e.g. from (Toro 1999), that each solution of the linear hyperbolic system (4) is given by a linear combination of the right eigenvectors, i.e. $Q_p = R_{pq} \nu_q$, we can compute the coefficients as $\nu_p = R_{pq}^{-1} Q_q^0$ via the initial amplitude vector. Applying this procedure for each of the three waves, we can synthesize the exact solution in the form

$$Q_p(x, y, z, t) = \sum_{l=1}^3 R_{pq}^{(l)} \nu_q^{(l)} \cdot e^{i \cdot (\omega_q^{(l)} t - k_x^{(l)} x - k_y^{(l)} y - k_z^{(l)} z)}. \quad (53)$$

In the convergence test, we use the superposition of three plane P-waves travelling perpendicular to each other. However, the symmetry axes of the anisotropic, orthorhombic material is tilted with respect to the coordinate system, i.e. the symmetry axes point into the directions $(1, 1, 1)$, $(-1, 1, 0)$ and $(-1, -1, 2)$, respectively. The initial condition at $t = 0$ is given by (53) using the combination of three right eigenvectors $R_{p1}^{(1)}$, $R_{p1}^{(2)}$ and $R_{p1}^{(3)}$ with the coefficients $\nu_1^{(1)} = \nu_1^{(2)} = \nu_1^{(3)} = 100$ and zero otherwise.

The total simulation time T is set to $T = 0.02s$. The CFL number is set in all computations to 50% of the stability limit $\frac{1}{2N+1}$ of Runge-Kutta DG schemes. For a thorough investigation of the linear stability properties of the ADER-DG schemes via a von Neumann analysis see (Dumbser 2005).

The numerical analysis to determine the convergence orders is performed on a sequence of tetrahedral meshes as shown in Figure 1. The mesh sequence is obtained by dividing the computational domain Ω into a number of subcubes, which are then subdivided into five tetrahedrons as shown in Figure 1. This way, the refinement is controlled by changing the number of subcubes in each dimension.

We can arbitrarily pick one of the variables of the system of the seismic wave equations (4) to numerically determine the convergence order of the used ADER-DG schemes. In Tables 2 and 3 we show the errors for the vertical velocity component w . The errors of the numerical solution Q_h with respect to the exact solution Q_e is measured in the L^∞ -norm and the continuous L^2 -norm

$$\|Q_h - Q_e\|_{L^2(\Omega)} = \left(\int_{\Omega} |Q_h - Q_e|^2 dV \right)^{\frac{1}{2}}, \quad (54)$$

where the integration is approximated by Gaussian integration which is exact for a polynomial degree twice that of the basis functions of the numerical scheme. The L^∞ -norm is approximated by the maximum error arising at any of these Gaussian integration points. The first column in both Tables 2 and 3 shows the mesh spacing h , represented by the maximum diameter of the circumscribed spheres of the tetrahedrons. The following four columns show the L^∞ and L^2 errors with the corresponding convergence orders \mathcal{O}_{L^∞} and \mathcal{O}_{L^2} determined by successively refined meshes. Furthermore, we present the total number N_d of degrees of freedom, which is a measure of required storage space during run-time and is given through the product of the number of total mesh elements and the number N_e of degrees of freedom per element. N_e depends on the order of the scheme, i.e. the degree N of the polynomial basis functions via $N_e(N) = \frac{1}{6}(N+1)(N+2)(N+3)$. In the last two columns we give the number I of iterations and the CPU times in seconds needed to reach the simulation time $T = 0.02s$ on a Pentium Xeon 3.6 GHz processor with 4GB of RAM.

In our convergence study, we compare two different numerical fluxes, i.e. the Rusanov flux as introduced in section 3 (see e.g. in (Toro 1999)) and a Godunov flux as given in detail in Appendix A. Figure 2 visualizes the convergence results of Tables 2 and 3 to demonstrate the dependence of the L^∞ error with respect to (a) mesh width h , (b) number of degrees of freedom N_d and (c) CPU time. With mesh refinement, for both choices of the numerical flux the higher order schemes converge faster as shown in Figure 2(a). Furthermore, Figure 2(b) demonstrates that higher order schemes reach a desired accuracy requiring a lower number of total degrees of freedom. The total number of degrees of freedom is the product of the number of mesh elements and the degrees of freedom per element. Therefore, obviously the increasing number of degrees of freedom of higher order schemes is over-compensated by the dramatic decrease of the number of required mesh elements to reach a certain error level. Also the CPU time comparisons in Figure 2(c) show that the higher order methods reach a desired error level in less computational time. We remark that in all three plots of Figure 2 we clearly show, that for very high accuracy, the higher order schemes with both, the Rusanov or Godunov fluxes, pay off due to their superior convergence properties.

Furthermore, we see in all plots that the Godunov flux is slightly more accurate than the Rusanov flux, which is due to well-known dissipative property of the Rusanov flux. Additionally, we want to remark, that with increasing order of the scheme the choice of the numerical flux seems to become less important. However, the Godunov flux always provides the more accurate results in less CPU time.

6 APPLICATION EXAMPLES

6.1 Heterogeneous Anisotropic Material

To validate the proposed ADER-DG scheme for anisotropic material in two space dimensions we show results of a heterogeneous anisotropic test case proposed by Carcione (1988) and Komatitsch *et al.* (2000). The computational domain $\Omega = [-32.5; 32.5]cm \times [-32.5; 32.5]cm$ is discretized by 37944 triangles with an average edge length of $0.5cm$, equal to the edge length of the square shaped elements used by Komatitsch *et al.* (2000). Along the boundary of Ω we use absorbing boundary conditions. The domain Ω contains two materials separated by a straight line at $x = 0$. On the one side ($x < 0$) we have an anisotropic (transversely isotropic) zinc crystal with the symmetry axis in y -direction, whereas on the other side ($x > 0cm$) we use an isotropic material. The corresponding material properties are given in Table 4. The source represents a point force at location $s = (-2cm, 0cm)$, i.e. $2cm$ from the material interface inside the anisotropic material and is acting in y -direction. The source time function is given by a Ricker wavelet with dominant frequency $f_0 = 170kHz$ and delay $t_0 = 6\mu s$ and acts on the vertical velocity component v with a maximum amplitude of $1 \cdot 10^{13}$. Seismograms are calculated at four different locations $r_i = (x_i, y_i)$, $i = 1, \dots, 4$, with $x_1 = -10.5cm$, $x_2 = -3.5cm$, $x_3 = -1.0cm$, $x_4 = 10.5cm$ and $y_i = -8cm$ for all $i = 1, \dots, 4$ in order to compare our results with those of Komatitsch *et al.* (2000). The simulation is carried out using a ADER-DG $\mathcal{O}6$ scheme, i.e. with polynomial basis functions of degree $N = 5$, and the Rusanov flux presented in Section 5. The time step size was $20.58ns$ such that the final

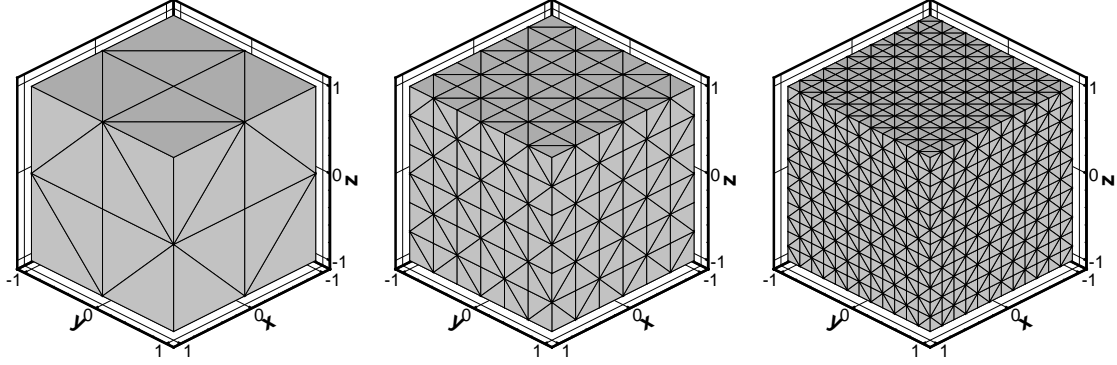


Figure 1. Sequence of discretizations of the computational domain Ω via regularly refined tetrahedral meshes, which are used for the numerical convergence analysis.

Table 2. Convergence rates of the vertical velocity component w of the ADER-DG $\mathcal{O}2$ up to ADER-DG $\mathcal{O}7$ schemes on tetrahedral meshes with anisotropic material and Rusanov flux.

h	L^∞	\mathcal{O}_{L^∞}	L^2	\mathcal{O}_{L^2}	N_d	I	CPU [s]
$1.44 \cdot 10^{-1}$	$1.3726 \cdot 10^{-1}$	—	$7.1719 \cdot 10^{-2}$	—	34560	28	20.4
$1.08 \cdot 10^{-1}$	$7.9448 \cdot 10^{-2}$	1.9	$4.0897 \cdot 10^{-2}$	2.0	81920	37	62.7
$8.66 \cdot 10^{-2}$	$5.1013 \cdot 10^{-2}$	2.0	$2.6304 \cdot 10^{-2}$	2.0	160000	46	150.4
$7.21 \cdot 10^{-2}$	$3.5739 \cdot 10^{-2}$	2.0	$1.8280 \cdot 10^{-2}$	2.0	276480	55	309.9
$1.44 \cdot 10^{-1}$	$9.6109 \cdot 10^{-3}$	—	$3.0957 \cdot 10^{-3}$	—	86400	46	44.8
$1.08 \cdot 10^{-1}$	$4.2996 \cdot 10^{-3}$	2.8	$1.3268 \cdot 10^{-3}$	2.9	204800	61	140.0
$8.66 \cdot 10^{-2}$	$2.0774 \cdot 10^{-3}$	3.3	$6.8331 \cdot 10^{-4}$	3.0	400000	76	334.7
$7.21 \cdot 10^{-2}$	$1.2533 \cdot 10^{-3}$	2.8	$3.7909 \cdot 10^{-4}$	3.2	691200	92	709.4
$2.16 \cdot 10^{-1}$	$2.4197 \cdot 10^{-3}$	—	$6.0996 \cdot 10^{-4}$	—	51200	43	21.5
$1.44 \cdot 10^{-1}$	$5.6764 \cdot 10^{-4}$	3.6	$1.1436 \cdot 10^{-4}$	4.1	172800	64	104.5
$1.08 \cdot 10^{-1}$	$1.6407 \cdot 10^{-4}$	4.3	$3.8141 \cdot 10^{-5}$	3.8	409600	85	322.6
$7.21 \cdot 10^{-2}$	$3.4818 \cdot 10^{-5}$	3.8	$7.4515 \cdot 10^{-6}$	4.0	1382400	128	1623.5
$4.33 \cdot 10^{-1}$	$4.3718 \cdot 10^{-3}$	—	$8.3266 \cdot 10^{-4}$	—	11200	28	3.4
$2.16 \cdot 10^{-1}$	$1.3161 \cdot 10^{-4}$	5.0	$2.2487 \cdot 10^{-5}$	5.2	89600	55	50.0
$1.44 \cdot 10^{-1}$	$1.7960 \cdot 10^{-5}$	4.9	$2.9100 \cdot 10^{-6}$	5.0	302400	82	248.7
$1.08 \cdot 10^{-1}$	$4.2391 \cdot 10^{-6}$	5.0	$7.1098 \cdot 10^{-7}$	4.9	716800	110	801.3
$8.66 \cdot 10^{-1}$	$1.7247 \cdot 10^{-2}$	—	$3.0907 \cdot 10^{-3}$	—	2240	17	0.5
$4.33 \cdot 10^{-1}$	$3.6214 \cdot 10^{-4}$	5.6	$5.2490 \cdot 10^{-5}$	5.9	17920	34	7.8
$2.16 \cdot 10^{-1}$	$6.1905 \cdot 10^{-6}$	5.9	$7.8147 \cdot 10^{-7}$	6.0	143360	67	118.8
$1.44 \cdot 10^{-1}$	$5.4051 \cdot 10^{-7}$	6.0	$6.5986 \cdot 10^{-8}$	6.1	483840	101	611.0
$8.66 \cdot 10^{-1}$	$2.5263 \cdot 10^{-3}$	—	$4.0569 \cdot 10^{-4}$	—	3360	20	1.2
$4.33 \cdot 10^{-1}$	$2.5296 \cdot 10^{-5}$	6.6	$2.8757 \cdot 10^{-6}$	7.1	26880	40	18.3
$2.88 \cdot 10^{-1}$	$1.5502 \cdot 10^{-6}$	6.9	$1.6396 \cdot 10^{-7}$	7.0	90720	60	91.8
$2.16 \cdot 10^{-1}$	$1.9551 \cdot 10^{-7}$	7.2	$2.1993 \cdot 10^{-8}$	7.0	215040	79	285.1

Table 3. Convergence rates of the vertical velocity component w of the ADER-DG $\mathcal{O}2$ up to ADER-DG $\mathcal{O}7$ schemes on tetrahedral meshes with anisotropic material and Godunov flux.

h	L^∞	\mathcal{O}_{L^∞}	L^2	\mathcal{O}_{L^2}	N_d	I	CPU [s]
$1.44 \cdot 10^{-1}$	$1.0041 \cdot 10^{-1}$	—	$5.4423 \cdot 10^{-2}$	—	34560	28	20.3
$1.08 \cdot 10^{-1}$	$5.8267 \cdot 10^{-2}$	1.9	$3.0369 \cdot 10^{-2}$	2.0	81920	37	63.3
$8.66 \cdot 10^{-2}$	$3.7871 \cdot 10^{-2}$	1.9	$1.9512 \cdot 10^{-2}$	2.0	160000	46	151.0
$7.21 \cdot 10^{-2}$	$2.5901 \cdot 10^{-2}$	2.1	$1.3477 \cdot 10^{-2}$	2.0	276480	55	310.2
$1.44 \cdot 10^{-1}$	$8.8110 \cdot 10^{-3}$	—	$2.7851 \cdot 10^{-3}$	—	86400	46	45.2
$1.08 \cdot 10^{-1}$	$3.9071 \cdot 10^{-3}$	2.8	$1.1894 \cdot 10^{-3}$	3.0	204800	61	138.6
$8.66 \cdot 10^{-2}$	$1.8371 \cdot 10^{-3}$	3.4	$6.1510 \cdot 10^{-4}$	3.0	400000	76	341.2
$7.21 \cdot 10^{-2}$	$1.1421 \cdot 10^{-3}$	2.6	$3.3983 \cdot 10^{-4}$	3.3	691200	92	703.3
$2.16 \cdot 10^{-1}$	$2.1082 \cdot 10^{-3}$	—	$5.3961 \cdot 10^{-4}$	—	51200	43	21.5
$1.44 \cdot 10^{-1}$	$4.8616 \cdot 10^{-4}$	3.6	$9.8006 \cdot 10^{-5}$	4.2	172800	64	107.7
$1.08 \cdot 10^{-1}$	$1.4123 \cdot 10^{-4}$	4.3	$3.3024 \cdot 10^{-5}$	3.8	409600	85	326.0
$7.21 \cdot 10^{-2}$	$3.0079 \cdot 10^{-5}$	3.8	$6.3742 \cdot 10^{-6}$	4.1	1382400	128	1620.8
$4.33 \cdot 10^{-1}$	$3.8588 \cdot 10^{-3}$	—	$7.3824 \cdot 10^{-4}$	—	11200	28	3.4
$2.16 \cdot 10^{-1}$	$1.1900 \cdot 10^{-4}$	5.0	$2.0750 \cdot 10^{-5}$	5.2	89600	55	51.0
$1.44 \cdot 10^{-1}$	$1.6555 \cdot 10^{-5}$	4.9	$2.6735 \cdot 10^{-6}$	5.0	302400	82	248.1
$1.08 \cdot 10^{-1}$	$3.8443 \cdot 10^{-6}$	5.1	$6.5261 \cdot 10^{-7}$	4.9	716800	110	799.5
$8.66 \cdot 10^{-1}$	$1.6633 \cdot 10^{-2}$	—	$2.9909 \cdot 10^{-3}$	—	2240	17	0.5
$4.33 \cdot 10^{-1}$	$3.2571 \cdot 10^{-4}$	5.7	$4.7736 \cdot 10^{-5}$	6.0	17920	34	7.8
$2.16 \cdot 10^{-1}$	$5.4583 \cdot 10^{-6}$	5.9	$7.0059 \cdot 10^{-7}$	6.1	143360	67	123.0
$1.44 \cdot 10^{-1}$	$4.7499 \cdot 10^{-7}$	6.0	$5.8732 \cdot 10^{-8}$	6.1	483840	101	606.7
$8.66 \cdot 10^{-1}$	$2.0000 \cdot 10^{-3}$	—	$3.4171 \cdot 10^{-4}$	—	3360	20	1.2
$4.33 \cdot 10^{-1}$	$2.2341 \cdot 10^{-5}$	6.5	$2.6403 \cdot 10^{-6}$	7.0	26880	40	18.1
$2.88 \cdot 10^{-1}$	$1.4003 \cdot 10^{-6}$	6.8	$1.5055 \cdot 10^{-7}$	7.1	90720	60	90.2
$2.16 \cdot 10^{-1}$	$1.7634 \cdot 10^{-7}$	7.2	$2.0326 \cdot 10^{-8}$	7.0	215040	79	281.4

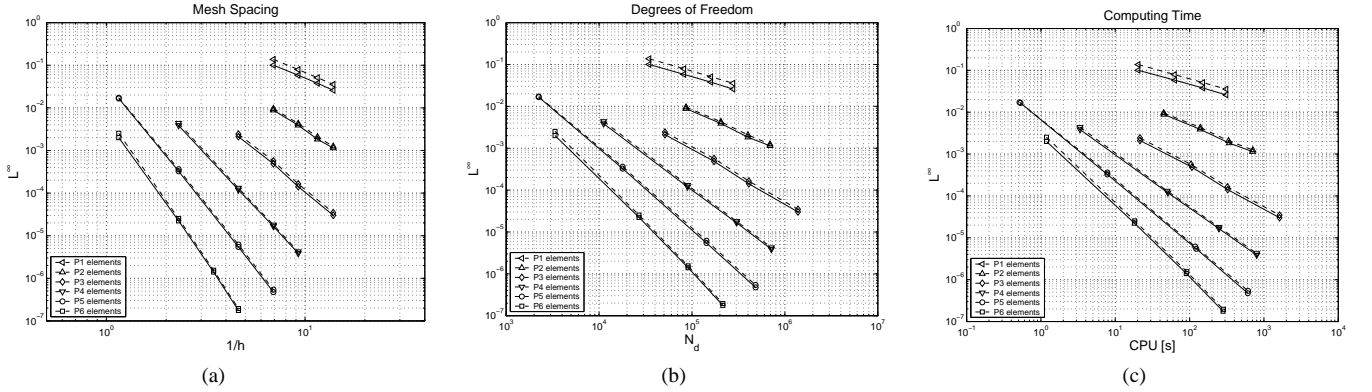

Figure 2. Visualization of the convergence results of the vertical velocity component w for the Rusanov flux (dashed) of Table 2 and the Godunov flux (solid) of Table 3. The L^∞ error is plotted versus (a) the mesh spacing h , (b) the number of degrees of freedom N_d and (c) the CPU time.

Table 4. Coefficients for the heterogeneous anisotropic model given in $[10^{10} N \cdot m^{-2}]$ for the anisotropic and isotropic materials. All other coefficients are zero. The material density ρ is given in $[kg \cdot m^{-3}]$.

	ρ	c_{11}	c_{12}	c_{22}	c_{66}
isotropic	7100	16.5	8.58	16.5	3.96
anisotropic	7100	16.5	5.00	6.2	3.96

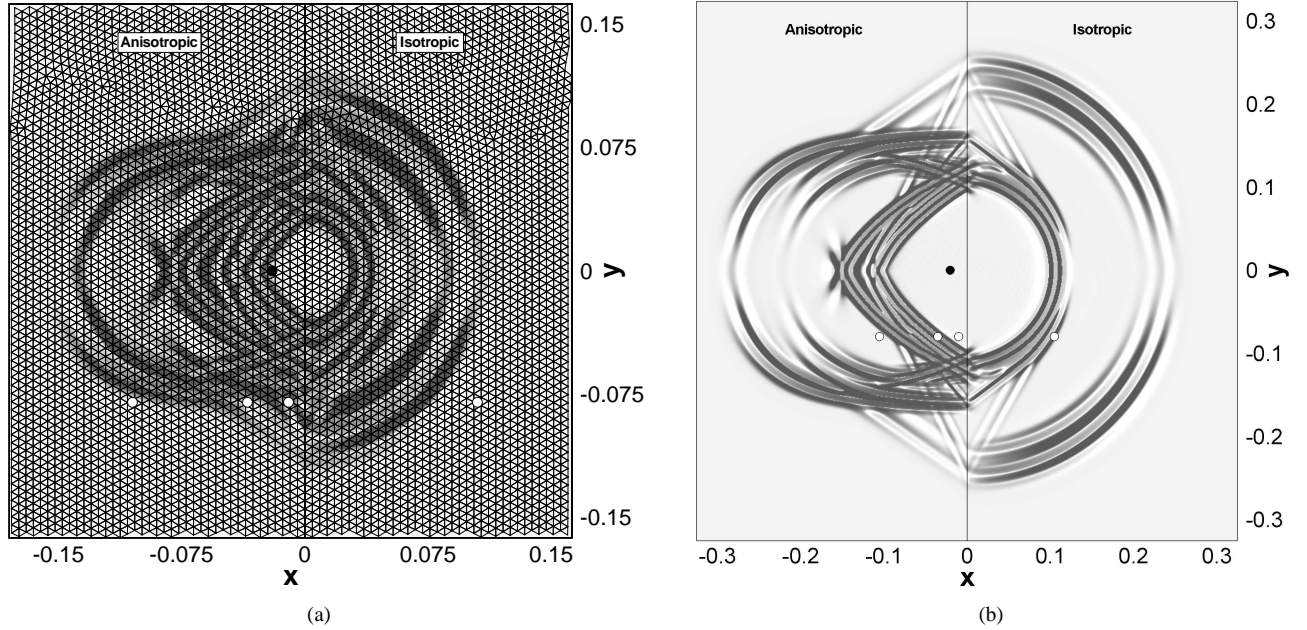


Figure 3. (a) Vertical velocity v and computational mesh in the zoomed region $[-0.18; 0.1625] \times [-0.1625; 0.1625]$ at $30\mu s$. The source location is indicated by a full (black) circle, the four receiver locations are indicated by empty (white) circles. (b) Vertical velocity v at $60\mu s$ with the whole computational domain. A variety of different phases can be identified. The source location is indicated by a full (black) circle, the four receiver locations are indicated by empty (white) circles.

simulation time $T = 100\mu s$ was reached after 4860 iterations.

Similar to (Komatitsch, Barnes & Tromp 2000) we illustrate two snapshots of the evolving wave field for a qualitative comparison. In Fig. 3(a) we show the vertical velocity component v after $30\mu s$ in a zoomed region together with the simulation mesh. Note, that the triangular elements are aligned with the material interface at $x = 0$. The locations of the source and the four receivers are also indicated by a full and empty circles, respectively. Fig. 3(b) illustrates the wave field of the velocity v after $60\mu s$ in the entire computational domain Ω together with the source and receiver locations. This visual comparison to the results of Komatitsch *et al.* (2000) shows, that the ADER-DG $\mathcal{O}6$ scheme resolves the same wave phases as described in detail in (Komatitsch, Barnes & Tromp 2000). The typical cuspidal triangular wave structures and the refracted waves at the interface are clearly visible.

The seismograms calculated with the ADER-DG $\mathcal{O}6$ scheme at the four receiver locations $r_i, i = 1, \dots, 4$, are plotted in Fig. 4 (solid line). The results obtained by Komatitsch *et al.* (2000) with the SEM of spatial order 6 are superimposed (dashed line). We remark, that these SEM seismograms are obtained by digitizing the seismograms presented by Komatitsch *et al.* (2000) and then scaling them, such that the maximum amplitude in each plot is identical since no information about the source amplitude was given by Komatitsch *et al.* (2000). The agreement is excellent, in particular for the first phases. However, very small time shifts can be observed at the last phase. Komatitsch *et al.* (2000) already recognized this phase shift in their seismograms compared to a FD fine grid reference solution and interpreted the differences as an effect of the staggered grid of the FD scheme. We mention, that the time shifts could also be due to their time stepping scheme, which is only second order accurate, whereas the ADER-DG $\mathcal{O}6$ scheme converges with order 6 in space *and* time, as confirmed in Table 2. We admit, that possible errors might have been introduced also due to the digitization of the SEM seismograms.

6.2 Transversely Isotropic Material with Tilted Symmetry Axis

To verify the accuracy of the proposed scheme for a fully three-dimensional problem we perform a computation of the test case proposed in (Komatitsch, Barnes & Tromp 2000) for a 3D transversely isotropic medium with tilted symmetry axis. We study a homogeneous material, in this case Mesaverde Clay shale, by applying a point source aligned with the material's symmetry axis. In the mentioned publication, the whole setup is tilted 30° in order to add complexity to the Hooke's tensor which in a cartesian system will now have a major number of non-zero entries. In our case, as the fluxes are performed in coordinate systems aligned with the face of the each tetrahedron, this added complexity is already present. However, to keep as close to the original work as possible, we also reproduce the tilted axis in our simulation. The source is a Ricker wavelet with $\nu_0 = 16Hz$ and $t_0 = 0.07s$. The computational domain is a cube of dimensions $2500m \times 2500m \times 2500m$ discretized with $48 \times 48 \times 48$ cubes, each subdivided in 5 tetrahedra, for a total of 552 960 elements. We choose to use an ADER-DG $\mathcal{O}6$ scheme, meaning that the variables are resolved with polynomials of degree $N = 5$ in space and time inside each element. Fluxes

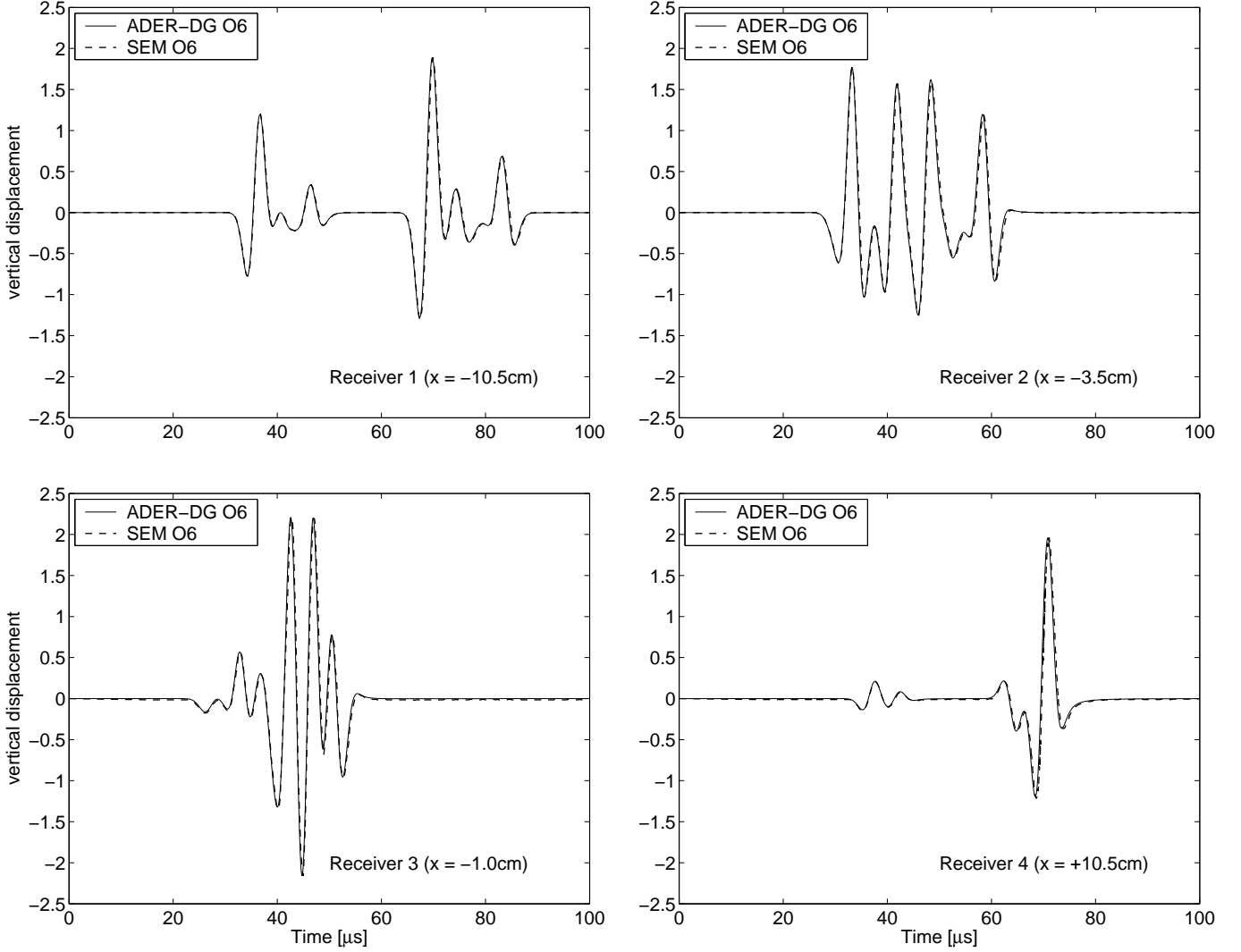


Figure 4. Seismograms.

Table 5. Coefficients for the transversely isotropic material (Mesaverde clay shale) given in $[10^9 N \cdot m^{-2}]$. All other coefficients are zero. The material density ρ is given in $[kg \cdot m^{-3}]$.

ρ	c_{11}	c_{12}	c_{13}	c_{22}	c_{23}	c_{33}	c_{44}	c_{55}	c_{66}
2590	66.6	19.7	39.4	66.6	39.4	39.9	10.9	10.9	23.45

used are of Godunov's type. The actual material parameters, in the symmetry axis aligned reference system, can be found in table 5. Notice that for a transversely isotropic material $c_{22} = c_{11}$, $c_{23} = c_{13}$ and $c_{55} = c_{44}$.

The source is placed at $(x, y, z) = (1250, 1562.5, 937.5) m$ and the receiver at $(x, y, z) = (1250, 1198.05, 1568.75) m$. Afterwards the whole mesh is translated along the vector $(x, y, z) = (10, 10, 10) m$ so that both source and receiver are inside elements and not at points. It is an important fact that in the ADER-DG formulation there is no need to make coincide sources and receivers to grid points. The time step size was $197.29 \mu s$ such that the final simulation time $T = 0.7 s$ was reached after 3548 iterations.

The results and comparisons with the analytical solution first derived in (Carcione, Kosloff, Behle & Seriani 1992) are shown in figure 6. We can see the excellent agreement between analytical and numerical solutions, where we can observe both the early qP wave followed by the stronger qSV wave. We also found, as in (Komatitsch, Barnes & Tromp 2000), a slight discrepancy in the amplitudes. Note also that we use absorbing boundaries in the outer faces of the cube, so that we don't get any reflected wave. For the computation of the numerical solution we needed approximately 11 hours of CPU time on 64 Intel Itanium2 64-bit 1.6-GHz processors with shared-memory.

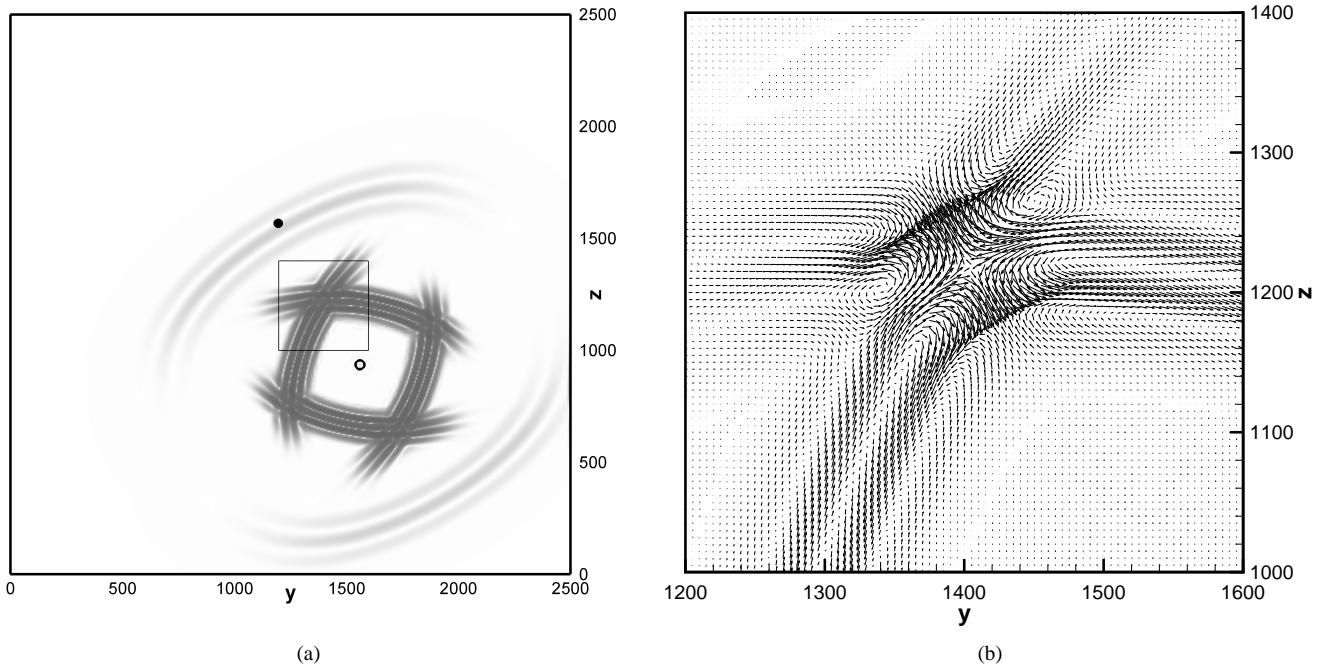


Figure 5. (a) Snapshot of the normal stress σ_{xx} at $t = 0.25s$ in the yz -plane at $x = 1250m$ (top). The source and receiver positions are indicated by the empty and full circles, respectively. The zoom region for Figure 5(b) is indicated by the box. (b) Vector field of the particle velocity at $t = 0.25s$ in the zoom region.

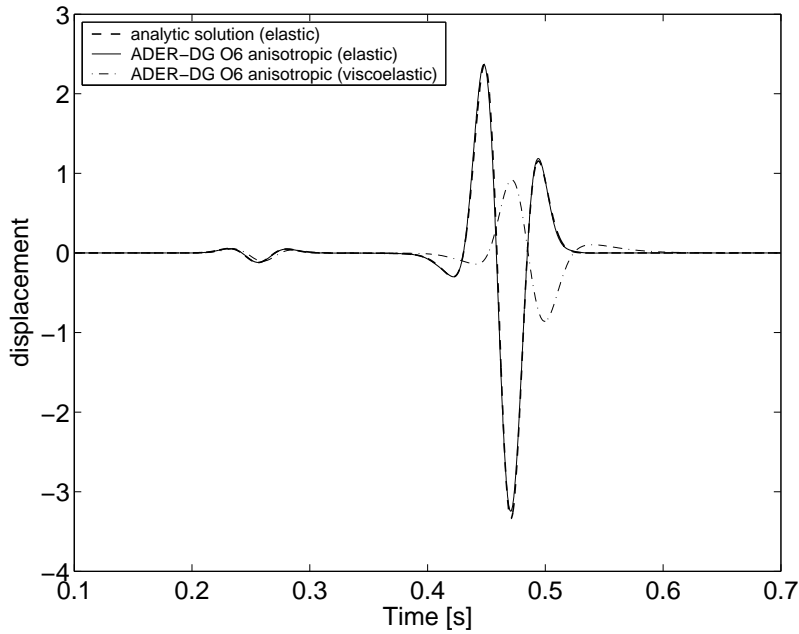


Figure 6. Numerical (solid) and analytical (dotted) displacements along the symmetry axis recorded at 728.9m from the source. The numerical solution is computed with an ADER-DG $\mathcal{O}6$ scheme and shows excellent agreement with the analytical solution

7 CONCLUSION

We have presented a high-order scheme for solving problems of seismic wave propagation for the anisotropic case on unstructured tetrahedral meshes. The ADER-DG method has proven to be very well suited for achieving highly accurate results in arbitrarily anisotropic materials. Two possible flux choices have been introduced and compared. Additionally a way to couple both anisotropic and viscoelastic effects has been developed together with the changes that this coupling has in the scheme’s explicit expression. The theoretical accuracy orders have

been achieved in convergence tests and a two medium-scale applications involving qP , qS_1 and qS_2 wave propagation in both homogenous and heterogeneous media have shown a very good agreement with results obtained with other methods for wave propagation and known analytical solutions.

We conclude that the ADER-DG method offers an excellent balance between flexibility and accuracy and in the future many applications could be performed involving more realistic setups, particularly in areas where a clear distinction between geometry- and anisotropy-caused phase splitting can be crucial, as is in cracked sedimentary layers or in studies of the upper mantle or oceanic crust. Future work will aim at exploring such complex cases, as well as comparisons between the performance of other known methods for anisotropic wave propagation and the method presented here.

8 ACKNOWLEDGMENT

The authors thank the European Research and Training Network SPICE (Seismic Wave Propagation in Complex Media: a European Network) as well as the DFG (Deutsche Forschungsgemeinschaft), as the work was supported through the Emmy Noether-program (KA 2281/1-1) and the DFG-CNRS research group FOR 508, Noise Generation in Turbulent Flows. Also to Dimitri Komatitsch for providing us with the analytical solution used in section 6 and to the super-computing facilities of the LRZ München for allowing us to use their clusters for the computation of the results shown in the present work.

REFERENCES

- Auld, B. A., 1990. *Acoustic Fields and Waves in Solids*, Vol. 1, Krieger Publishing Company, Malabar, Florida.
- Backus, G.E., 1962. Long-wave elastic anisotropy produced by horizontal layering, *J. Geophys. Res.*, **67**, 4427-4440.
- Bond, W.L., 1976. *Crystal Technology*, Wiley, New York.
- Browaeyns, J.T. & Chevrot, S., 2004. Decomposition of the elastic tensor and geophysical applications, *Geophys. J. Int.*, **159**, 667-678.
- Cara, M., 2002. Seismic Anisotropy, in *International Handbook of Earthquake and Engineering Seismology*, Part A, Eds. Lee, W.H.K., Kanamori, H., Jennings, P.C. & Kisslinger, C., Academic Press, London.
- Carcione, J.M., 1994. The wave equation in generalised coordinates, *Geophysics*, **59**, 1911-1919.
- Carcione, J. M., 1995. Constitutive model and wave equations for linear, viscoelastic, anisotropic media, *Geophysics*, **60**, 537-548.
- Carcione, J.M., 2002. Wave Fields in Real Media: Wave Propagation in Anisotropic, Anelastic and Porous Media, in *Handbook of Geophysical Exploration, Seismic Exploration*, Vol. 31, Eds. Helbig, K. & Treitel, S., Pergamon, Oxford.
- Carcione, J.M. & Cavallini, F., 1994. A rheological model for anelastic anisotropic media with applications to seismic wave propagation, *Geophys. J. Int.*, **119**, 338-348.
- Carcione, J.M., Kosloff, D., Behle, A. & Seriani, G., 1992. A spectral scheme for wave propagation simulation in 3-D elastic anisotropic media, *Geophysics*, **57**, 1593-1607.
- Carcione, J.M., Kosloff, D. & Kosloff, R., 1988. Wave propagation simulation in an elastic anisotropic (transversely isotropic) solid, *Q. J. Mech. Appl. Math.*, **41**, 319-345.
- Červený, V., 1972. Seismic rays and ray intensities in inhomogeneous anisotropic media, *Geophys. J. Roy. Astr. Soc.*, **29**, 1-13.
- Crampin, S., 1981. A review of wave motion in anisotropic and cracked elastic media, *Wave Motion*, **3**, 343-391.
- Crampin, S., Chesnokov, E.M. & Hipkin, R.G., 1984. Seismic anisotropy - The state of the art II, *Geophys. J. Roy. Astr. Soc.*, **76**, 1-16.
- Dumbser, M., 2005. *Arbitrary High Order Schemes for the Solution of Hyperbolic Conservation Laws in Complex Domains*, Shaker Verlag, Aachen.
- Dumbser, M. & Käser, M., 2006. An Arbitrary High Order Discontinuous Galerkin Method for Elastic Waves on Unstructured Meshes II: The Three-Dimensional Isotropic Case. to appear in *Geophys. J. Int.*
- Dumbser, M., Käser, M. & de la Puente, J., 2006. Arbitrary High Order Finite Volume Schemes for Seismic Wave Propagation on Unstructured Meshes in 2D and 3D, submitted
- Emmerich, H. & Korn, M., 1987. Incorporation of attenuation into time-domain computations of seismic wave fields, *Geophysics*, **52**, 1252-1264.
- Fornberg, B., 1996. *A Practical Guide to Pseudospectral Methods*, Cambridge University Press, Cambridge.
- Gao, H. & Zhang, J., 2006. Parallel 3-D simulation of seismic wave propagation in heterogeneous anisotropic media: a grid method approach, *Geophys. J. Int.*, **165**, 875-888.
- Helbig, K., 1994. Foundations of anisotropy for exploration seismics, in *Handbook of Geophysical Exploration, Section I, Seismic Exploration*, Vol. 22, Eds. Helbig, K. & Treitel, S., Pergamon, Oxford.
- Hung, S.H. & Forsyth, D.W., 1998. Modelling anisotropic wave propagation in oceanic inhomogeneous structures using the parallel multidomain pseudospectral method, *Geophys. J. Int.*, **133**, 726-740.
- Igel, H., 1999. Wave propagation in three-dimensional spherical sections by the Chebyshev spectral method, *Geophys. J. Int.*, **136**, 559-566.
- Igel, H., Mora, P. & Rioulet, B., 1995. Anisotropic wave propagation through finite-difference grids, *Geophysics*, **60**, 1203-1216.
- Käser, M. & Dumbser, M., 2006. An Arbitrary High Order Discontinuous Galerkin Method for Elastic Waves on Unstructured Meshes I: The Two-Dimensional Isotropic Case with External Source Terms, *Geophys. J. Int.*, **166**, 855-877.
- Käser, M., Dumbser, M., de la Puente, J. & Igel, H., 2006. An Arbitrary High Order Discontinuous Galerkin Method for Elastic Waves on Unstructured Meshes III: Viscoelastic Attenuation, to appear in *Geophys. J. Int.*
- Komatitsch, D. & Vilotte, J.P., 1998. The spectral-element method: an efficient tool to simulate the seismic response of 2D and 3D geological structures, *Bull. Seism. Soc. Am.*, **88**, 368-392.
- Komatitsch, D. & Tromp, J., 1999. Introduction to the spectral-element method for 3-D seismic wave propagation, *Geophys. J. Int.*, **139**, 806-822.
- Komatitsch, D., Barnes, C. & Tromp, J., 2000. Simulation of anisotropic wave propagation based upon a spectral element method, *Geophysics*, **65**, 1251-1260.
- Komatitsch, D. & Tromp, J., 2002. Spectral-element simulations of global seismic wave propagation - I. Validation, *Geophys. J. Int.*, **149**, 390-412.
- LeVeque, R.L., 2002. *Finite Volume Methods for Hyperbolic Problems*, Cambridge University Press, Cambridge, UK.

- Madariaga, R., 1976. Dynamics of an expanding circular fault. *Bull. Seism. Soc. Am.*, **65**, 163-182.
- Moczo, P., Kristek, J. & Halada, L., 2004. *The Finite Difference Method for Seismologists. An Introduction*, Comenius University, Bratislava, available at <http://www.spice-rtn.org/>
- Mora, P., 1989. Modeling anisotropic seismic waves in 3-D, *59th Ann. Int. Mtg Exploration Geophysicists, expanded abstracts*, 1039-1043.
- Nye, J.F., 1985. *Physical Properties of Crystals*, Oxford University Press, London.
- Okaya, D.A. & McEvelly, T.V., 2003. Elastic wave propagation in anisotropic crustal material possessing arbitrary internal tilt, *Geophys. J. Int.*, **153**, 344-358.
- Saenger, E. H. & Bohlen, T., 2004. Finite-difference modelling of viscoelastic and anisotropic wave propagation using the rotated staggered grid, *Geophysics*, **69**, 583-591.
- Seriani, G., Priolo, E. & Pregarz, A., 1995. Modelling waves in anisotropic media by a spectral element method, in Third international conference on mathematical and numerical aspects of wave propagation, Ed. Cohen, G., *Soc. Ind. Appl. Math.*, 289-298.
- Sharma, M.D. & Garg, N., 2006. Wave velocities in a pre-stressed anisotropic elastic medium, *J. Earth Syst. Sci.*, **115**, No. 2, 257-265.
- Song, L.P., Every, A.G. & Wright, C., 2001. Linearized approximations for phase velocities of elastic waves in weakly anisotropic media, *J. Phys. D: Appl. Phys.*, **34**, 2052-2062.
- Stein, S., Wysession, M., 2003. *An Introduction to Seismology, Earthquakes, and Earth Structure*, Blackwell Publishing.
- Tessmer, E., 1995. 3-D Seismic modelling of general material anisotropy in the presence of the free surface by a Chebyshev spectral method, *Geophys. J. Int.*, **121**, 557-575.
- Tessmer, E. & Kosloff, D., 1994. 3-D Elastic modelling with surface topography by a Chebyshev spectral method, *Geophysics*, **59**, 464-473.
- Thomsen, L., 1986. Weak elastic anisotropy, *Geophysics*, **51**, 1954-1966.
- Toro, E.F., 1999. *Riemann Solvers and Numerical Methods for Fluid Dynamics*, Springer, Berlin.
- Virieux, J., 1984. SH-wave propagation in heterogeneous media: Velocity-stress finite-difference method, *Geophysics*, **49**, 1933-1942.
- Virieux, J., 1986. P-SV wave propagation in heterogeneous media: Velocity-stress finite-difference method, *Geophysics*, **51**, 889-901.

APPENDIX A: GODUNOV FLUX FOR ANISOTROPIC MATERIAL

The flux formulation we use requires the use of numerical viscosity to stabilize the scheme. This term can have different structure depending on the flux type. The Godunov's (also referred as Roe's) method ensures the theoretical minimum viscosity by the use of the matrix $|A|$ as a stabilizing factor. This matrix in practice decomposes the characteristic waves at an interface into purely outgoing and purely incoming. It has formally the expression

$$|A| = R|\Lambda|R^{-1}, \quad (\text{A1})$$

where $|A|$ is a diagonal matrix containing the absolute values of the eigenvectors of the jacobian A , expressed at the interface and oriented to the normal of it, and R is the matrix of right eigenvectors of A . Both R and Λ are assumed to have the same ordering, meaning that the first column of R corresponds to the first eigenvalue of A appearing in Λ , the second column of R corresponds to the second diagonal element in Λ and so on. The non-zero eigenvalues of A , for both elastic and viscoelastic cases, can be found by solving the cubic equation system (18). In the following we will always assume a strictly descending ordering of the eigenvalues that compose Λ and R .

A1 Computation of the elastic part of $|A|$

If we assume a general shape of the right eigenvectors $\vec{R}_i = (r_i^1, r_i^2, r_i^3, r_i^4, r_i^5, r_i^6, r_i^7, r_i^8, r_i^9)^T$, the eigendecomposition equation $A\vec{R}_i = \alpha_i\vec{R}_i$ leads us to the explicit 9 equations

$$\begin{aligned} c_{11}r_i^7 + c_{16}r_i^8 + c_{15}r_i^9 &= \alpha_i r_i^1 & c_{12}r_i^7 + c_{26}r_i^8 + c_{25}r_i^9 &= \alpha_i r_i^2 & c_{13}r_i^7 + c_{36}r_i^8 + c_{35}r_i^9 &= \alpha_i r_i^3 \\ c_{16}r_i^7 + c_{66}r_i^8 + c_{56}r_i^9 &= \alpha_i r_i^4 & c_{14}r_i^7 + c_{46}r_i^8 + c_{45}r_i^9 &= \alpha_i r_i^5 & c_{15}r_i^7 + c_{56}r_i^8 + c_{55}r_i^9 &= \alpha_i r_i^6 \\ \frac{r_i^1}{\rho} &= \alpha_i r_i^7 & \frac{r_i^4}{\rho} &= \alpha_i r_i^8 & \frac{r_i^6}{\rho} &= \alpha_i r_i^9 \end{aligned} \quad (\text{A2})$$

of which 3 are dependant on the rest and the other six can be expressed in compact form as the following homogeneous linear system

$$\begin{pmatrix} X & c_{16} & c_{15} \\ c_{16} & Y & c_{56} \\ c_{15} & c_{56} & Z \end{pmatrix} \begin{pmatrix} r_i^7 \\ r_i^8 \\ r_i^9 \end{pmatrix} = \begin{pmatrix} 0 \\ 0 \\ 0 \end{pmatrix}, \quad (\text{A3})$$

with $X = c_{11} - \alpha_i^2 \rho$, $Y = c_{66} - \alpha_i^2 \rho$ and $Z = c_{55} - \alpha_i^2 \rho$, being α_i the eigenvalues. Note that this is exactly the Kelvin-Christoffel equation for anisotropic media which can be obtained from plane-wave analysis (Carcione 2002). However this equation appears here naturally from an eigendecomposition of the jacobians of our scheme (5). The solution of the linear system (A2) for the $i = 1, \dots, 9$ values completely defines the 9 right eigenvectors. The fact that the matrix of system (A3) has always zero determinant (equation (18) assures this) makes certain that we will always have non-trivial solutions. Knowing the values of r_i^7 , r_i^8 and r_i^9 we can use (A2) to obtain the rest of \vec{R}_i . Finally we would obtain the right eigenvector matrix

$$R = \begin{pmatrix} r_1^1 & r_1^2 & r_1^3 & 0 & 0 & 0 & -r_3^1 & -r_2^1 & -r_1^1 \\ r_1^2 & r_2^2 & r_3^2 & 1 & 0 & 0 & -r_3^2 & -r_2^2 & -r_1^2 \\ r_1^3 & r_2^3 & r_3^3 & 0 & 1 & 0 & -r_3^3 & -r_2^3 & -r_1^3 \\ r_1^4 & r_2^4 & r_3^4 & 0 & 0 & 0 & -r_3^4 & -r_2^4 & -r_1^4 \\ r_1^5 & r_2^5 & r_3^5 & 0 & 0 & 1 & -r_3^5 & -r_2^5 & -r_1^5 \\ r_1^6 & r_2^6 & r_3^6 & 0 & 0 & 0 & -r_3^6 & -r_2^6 & -r_1^6 \\ r_1^7 & r_2^7 & r_3^7 & 0 & 0 & 0 & r_3^7 & r_2^7 & r_1^7 \\ r_1^8 & r_2^8 & r_3^8 & 0 & 0 & 0 & r_3^8 & r_2^8 & r_1^8 \\ r_1^9 & r_2^9 & r_3^9 & 0 & 0 & 0 & r_3^9 & r_2^9 & r_1^9 \end{pmatrix}, \quad (\text{A4})$$

where the eigenvectors 4 to 6 are a choice. For the left eigenvectors, defined $\vec{L}_i = (l_i^1, l_i^2, l_i^3, l_i^4, l_i^5, l_i^6, l_i^7, l_i^8, l_i^9)$, there exists the eigendecomposition $\vec{L}_i A = \alpha_i \vec{L}_i$ for which we can explicitly write a series of equations which are

$$\begin{aligned} c_{11}l_i^1 + c_{16}l_i^4 + c_{15}l_i^6 &= \alpha_i l_i^7 & c_{16}l_i^1 + c_{66}l_i^4 + c_{56}l_i^6 &= \alpha_i l_i^8 & c_{15}l_i^1 + c_{56}l_i^4 + c_{55}l_i^6 &= \alpha_i l_i^9 \\ l_i^2 &= 0 & l_i^3 &= 0 & l_i^5 &= 0 \\ \frac{l_i^7}{\rho} &= \alpha_i l_i^1 & \frac{l_i^8}{\rho} &= \alpha_i l_i^4 & \frac{l_i^9}{\rho} &= \alpha_i l_i^6 \end{aligned} \quad (\text{A5})$$

which similarly as in the R case, can be expressed compactly by the homogeneous system

$$\begin{pmatrix} X & c_{16} & c_{15} \\ c_{16} & Y & c_{56} \\ c_{15} & c_{56} & Z \end{pmatrix} \begin{pmatrix} l_i^1 \\ l_i^4 \\ l_i^6 \end{pmatrix} = \begin{pmatrix} 0 \\ 0 \\ 0 \end{pmatrix}, \quad (\text{A6})$$

where we can observe the symmetries between the left and right eigenvectors, which are $r_i^1 = l_i^7, r_i^4 = l_i^8, r_i^6 = l_i^9, r_i^7 = l_i^1, r_i^8 = l_i^4$ and $r_i^9 = l_i^6$. This allows us to find left eigenvectors of A , but to avoid scaling problems, we want that left eigenvectors such that $L = R^{-1}$ holds. To this goal we set up the normalization

$$\left(\frac{\vec{L}_i}{2\alpha_i S_i} \right) \vec{R}_i = 1, \quad (\text{A7})$$

of which we can conclude that $S_i = \rho \left[(r_i^7)^2 + (r_i^8)^2 + (r_i^9)^2 \right]$. Now we can finally write down the L matrix of left eigenvectors as a function exclusively of the right eigenvectors' components with the following expression

$$L = R^{-1} = \begin{pmatrix} \frac{r_1^7}{2\alpha_1 S_1} & 0 & 0 & \frac{r_1^8}{2\alpha_1 S_1} & 0 & \frac{r_1^9}{2\alpha_1 S_1} & \frac{r_1^1}{2\alpha_1 S_1} & \frac{r_1^4}{2\alpha_1 S_1} & \frac{r_1^6}{2\alpha_1 S_1} \\ \frac{r_2^7}{2\alpha_2 S_2} & 0 & 0 & \frac{r_2^8}{2\alpha_2 S_2} & 0 & \frac{r_2^9}{2\alpha_2 S_2} & \frac{r_2^1}{2\alpha_2 S_2} & \frac{r_2^4}{2\alpha_2 S_2} & \frac{r_2^6}{2\alpha_2 S_2} \\ \frac{r_3^7}{2\alpha_3 S_3} & 0 & 0 & \frac{r_3^8}{2\alpha_3 S_3} & 0 & \frac{r_3^9}{2\alpha_3 S_3} & \frac{r_3^1}{2\alpha_3 S_3} & \frac{r_3^4}{2\alpha_3 S_3} & \frac{r_3^6}{2\alpha_3 S_3} \\ 0 & 1 & 0 & 0 & 0 & 0 & 0 & 0 & 0 \\ 0 & 0 & 1 & 0 & 0 & 0 & 0 & 0 & 0 \\ 0 & 0 & 0 & 0 & 1 & 0 & 0 & 0 & 0 \\ -\frac{r_3^7}{2\alpha_3 S_3} & 0 & 0 & -\frac{r_3^8}{2\alpha_3 S_3} & 0 & -\frac{r_3^9}{2\alpha_3 S_3} & \frac{r_3^1}{2\alpha_3 S_3} & \frac{r_3^4}{2\alpha_3 S_3} & \frac{r_3^6}{2\alpha_3 S_3} \\ -\frac{r_2^7}{2\alpha_2 S_2} & 0 & 0 & -\frac{r_2^8}{2\alpha_2 S_2} & 0 & -\frac{r_2^9}{2\alpha_2 S_2} & \frac{r_2^1}{2\alpha_2 S_2} & \frac{r_2^4}{2\alpha_2 S_2} & \frac{r_2^6}{2\alpha_2 S_2} \\ -\frac{r_1^7}{2\alpha_1 S_1} & 0 & 0 & -\frac{r_1^8}{2\alpha_1 S_1} & 0 & -\frac{r_1^9}{2\alpha_1 S_1} & \frac{r_1^1}{2\alpha_1 S_1} & \frac{r_1^4}{2\alpha_1 S_1} & \frac{r_1^6}{2\alpha_1 S_1} \end{pmatrix}, \quad (\text{A8})$$

where the eigenvectors 4 to 6 are a choice. We can now finally apply the equation (A1) and, without loss of generality, define $\bar{r}_j^i = \frac{r_j^i}{\sqrt{S_i}}$ to get the expression of $|A|$ as

$$|A| = \sum_{i=1}^3 \begin{pmatrix} \bar{r}_i^1 \bar{r}_i^7 & 0 & 0 & \bar{r}_i^1 \bar{r}_i^8 & 0 & \bar{r}_i^1 \bar{r}_i^9 & 0 & 0 & 0 \\ \bar{r}_i^2 \bar{r}_i^7 & 0 & 0 & \bar{r}_i^2 \bar{r}_i^8 & 0 & \bar{r}_i^2 \bar{r}_i^9 & 0 & 0 & 0 \\ \bar{r}_i^3 \bar{r}_i^7 & 0 & 0 & \bar{r}_i^3 \bar{r}_i^8 & 0 & \bar{r}_i^3 \bar{r}_i^9 & 0 & 0 & 0 \\ \bar{r}_i^4 \bar{r}_i^7 & 0 & 0 & \bar{r}_i^4 \bar{r}_i^8 & 0 & \bar{r}_i^4 \bar{r}_i^9 & 0 & 0 & 0 \\ \bar{r}_i^5 \bar{r}_i^7 & 0 & 0 & \bar{r}_i^5 \bar{r}_i^8 & 0 & \bar{r}_i^5 \bar{r}_i^9 & 0 & 0 & 0 \\ \bar{r}_i^6 \bar{r}_i^7 & 0 & 0 & \bar{r}_i^6 \bar{r}_i^8 & 0 & \bar{r}_i^6 \bar{r}_i^9 & 0 & 0 & 0 \\ 0 & 0 & 0 & 0 & 0 & 0 & \bar{r}_i^1 \bar{r}_i^7 & \bar{r}_i^1 \bar{r}_i^8 & \bar{r}_i^1 \bar{r}_i^9 \\ 0 & 0 & 0 & 0 & 0 & 0 & \bar{r}_i^4 \bar{r}_i^7 & \bar{r}_i^4 \bar{r}_i^8 & \bar{r}_i^4 \bar{r}_i^9 \\ 0 & 0 & 0 & 0 & 0 & 0 & \bar{r}_i^6 \bar{r}_i^7 & \bar{r}_i^6 \bar{r}_i^8 & \bar{r}_i^6 \bar{r}_i^9 \end{pmatrix}. \quad (\text{A9})$$

Notice that for obtaining the numerical value of the entries of (A9) we only need to know the 3 positive eigenvalues and their corresponding 3 solutions of the system in (A3). The remaining r_j^i values are obtained explicitly from using the expressions in (A2). Notice that only material values are involved in the whole $|A|$ computation, so that the values we compute don't change with time.

A2 Computation of the anelastic part of $|A|$

The anelastic part of $|A|$ can be also found by a similar procedure. Let's consider the general case in which we have n attenuating mechanisms. For each attenuating mechanism we introduce 6 new eigenvectors and eigenvalues. However the new eigenvalues have value zero so that, following our decreasing ordering, the eigenvalues are $\alpha_1 = -\alpha_{9+6n}, \alpha_2 = -\alpha_{8+6n}, \alpha_3 = -\alpha_{7+6n}$ and $\alpha_i = 0$ for $i = 4, \dots, 6 + 6n$. The right and left eigenvectors will now have the shape

$$\begin{aligned} \vec{R}_i &= \left(\bar{r}_i^1, \bar{r}_i^2, \bar{r}_i^3, \bar{r}_i^4, \bar{r}_i^5, \bar{r}_i^6, \bar{r}_i^7, \bar{r}_i^8, \bar{r}_i^9, \frac{\omega_1 \bar{r}_i^7}{\alpha_i}, 0, 0, \frac{\omega_1 \bar{r}_i^8}{2\alpha_i}, 0, \frac{\omega_1 \bar{r}_i^9}{2\alpha_i}, \dots, \frac{\omega_n \bar{r}_i^7}{\alpha_i}, 0, 0, \frac{\omega_n \bar{r}_i^8}{2\alpha_i}, 0, \frac{\omega_n \bar{r}_i^9}{2\alpha_i} \right)^T, \\ \vec{L}_i &= (\bar{r}_i^7, 0, 0, \bar{r}_i^8, 0, \bar{r}_i^9, \bar{r}_i^1, \bar{r}_i^4, \bar{r}_i^6, 0, 0, 0, 0, 0, \dots, 0, 0, 0, 0, 0), \end{aligned} \quad (\text{A10})$$

which brings us the possibility of building up the blocks for the ℓ -th mechanism, analogous to that of equation (36) for the A case, which are

$$A_\ell^{\parallel} = \omega_\ell \sum_{i=1}^3 \begin{pmatrix} \frac{\bar{r}_i^7 \bar{r}_i^7}{\alpha_i} & 0 & 0 & \frac{\bar{r}_i^7 \bar{r}_i^8}{\alpha_i} & 0 & \frac{\bar{r}_i^7 \bar{r}_i^9}{\alpha_i} & 0 & 0 & 0 \\ 0 & 0 & 0 & 0 & 0 & 0 & 0 & 0 & 0 \\ 0 & 0 & 0 & 0 & 0 & 0 & 0 & 0 & 0 \\ \frac{\bar{r}_i^7 \bar{r}_i^8}{2\alpha_i} & 0 & 0 & \frac{\bar{r}_i^8 \bar{r}_i^8}{2\alpha_i} & 0 & \frac{\bar{r}_i^8 \bar{r}_i^9}{2\alpha_i} & 0 & 0 & 0 \\ 0 & 0 & 0 & 0 & 0 & 0 & 0 & 0 & 0 \\ \frac{\bar{r}_i^7 \bar{r}_i^9}{2\alpha_i} & 0 & 0 & \frac{\bar{r}_i^8 \bar{r}_i^9}{2\alpha_i} & 0 & \frac{\bar{r}_i^9 \bar{r}_i^9}{2\alpha_i} & 0 & 0 & 0 \end{pmatrix}, \quad (\text{A11})$$

from which we can recover the isotropic case by setting $(r_1^7, r_1^8, r_1^9) = (1, 0, 0)$, $(r_2^7, r_2^8, r_2^9) = (0, 1, 0)$ and $(r_3^7, r_3^8, r_3^9) = (0, 0, 1)$.